Ribosome stalling caused by the Argonaute-microRNA-SGS3 complex regulates the production of secondary siRNAs in plants

Hiro-oki Iwakawa[1,2,*], Andy Y.W. Lam[1,3], Akira Mine[2,4,5], Tomoya Fujita[6,7], Kaori Kiyokawa[1], Manabu Yoshikawa[8], Atsushi Takeda[4,5], Shintaro Iwasaki[3,6], Yukihide Tomari[1,3].

[1] Laboratory of RNA Function, Institute for Quantitative Biosciences, The University of Tokyo, Bunkyo-ku, Tokyo 113-0032, Japan.

[2]JST, PRESTO, Saitama 332-0012, Japan.

[3]Department of Computational Biology and Medical Sciences, Graduate School of Frontier Sciences, The University of Tokyo, Bunkyo-ku, Tokyo 113-0032, Japan.

[4]Ritsumeikan Global Innovation Research Organization, Ritsumeikan University, Kusatsu, Shiga 525-8577, Japan.

[5]Department of Biotechnology, Graduate School of Life Sciences, Ritsumeikan University, Shiga 525-8577, Japan.

[6]RNA Systems Biochemistry Laboratory, RIKEN Cluster for Pioneering Research, Wako, Saitama, 351-0198 Japan.

[7]School of Life Science and Technology, Tokyo Institute of Technology, Yokohama, Kanagawa, 226-8503 Japan.

[8]Division of Plant and Microbial Sciences, Institute of Agrobiological Sciences, National Agriculture and Food Research Organization, 2-1-2 Kannondai Tsukuba, Ibaraki 305-

8602, Japan.

*Correspondence: iwakawa@iqb.u-tokyo.ac.jp (H.-o.I)

Abstract

The path of ribosomes on mRNAs can be impeded by various obstacles. One such example is halting of ribosome movement by microRNAs, though the exact mechanism and physiological role remain unclear. Here, we find that ribosome stalling caused by the Argonaute-microRNA-SGS3 complex regulates the production of secondary small interfering RNAs (siRNAs) in plants. We show that the double-stranded RNA-binding protein SGS3 directly interacts with the 3′ end of the microRNA in an Argonaute protein, resulting in ribosome stalling. Importantly, microRNA-mediated ribosome stalling positively correlates with efficient production of secondary siRNAs from target mRNAs. Our results illustrate a role for paused ribosomes in regulation of small RNA function that may have broad biological implications across the plant kingdom.

Main

Ribosome movement can be interrupted by various factors including rare codons, special RNA structures and specific amino acid sequences called ribosome arrest peptides (Ito and Chiba, 2013; Schuller and Green, 2018). Although the physiological roles of such impediments are unclear, growing evidence indicates that ribosome stalling has diverse functions, including ER stress response, monitoring protein secretion, feedback regulation of methionine biosynthesis, quality control of mRNAs, and folding of nascent peptide chains (Ito and Chiba, 2013; Inada, 2017; Stein et al., 2019).

microRNAs (miRNAs) can cause ribosome stalling as well as inhibition of translation initiation, target RNA degradation or cleavage (Fabian et al., 2010; Iwakawa and Tomari, 2013; Iwakawa and Tomari, 2015; Hou et al., 2016; Li et al., 2016; Bazin et al., 2017; Zhang et al., 2018). To pause ribosomes, miRNAs need to form RNA-induced silencing complexes (RISCs) with Argonaute (AGO) protein, and extensively base-pair within the coding sequence (CDS) of the target mRNA (Iwakawa and Tomari, 2013; Hou et al., 2016; Zhang et al., 2018). However, these requirements are not sufficient for ribosome stalling in plants; although many plant miRNAs have their cleavable targets with perfect or near perfect complementary binding sites in CDS, only a few miRNA binding sites can induce ribosome stalling *in vivo* (Hou et al., 2016). Thus, unknown elements other than RISC binding should be required for miRNA-mediated ribosome pausing.

The biological function of the miRNA-mediated ribosome stalling also remains unclear. One plausible role of the miRNA-mediated ribosome stalling is inhibition of

functional protein synthesis (Iwakawa and Tomari, 2013; Iwakawa and Tomari, 2015; Zhang et al., 2018). However, given the diverse functions of stalled ribosomes as mentioned above, miRNA-mediated ribosome pausing may have a role other than translation repression.

Here, we show that a dsRNA binding protein, SGS3, is a key determinant of miRNA-mediated ribosome stalling. SGS3 forms a complex on dsRNA protruding from the miR390-AGO7-target complex. These mechanisms also operate in the context of a distinct 22-nucleotide miRNA-AGO1-RISC complex. Importantly, we find that SGS3 and miRNA-mediated ribosome stalling positively correlates with efficient amplification of RNA silencing, suggesting a new role of ribosome pausing beyond inhibition of protein synthesis.

Results

The dsRNA-binding protein SGS3 is a specific enhancer for microRNA-mediated ribosome stalling

We first sought to find the miRNA-mediated ribosome stalling positions. To do this, we performed ribosome profiling, an approach that is based on sequencing of ribosome-protected footprints after RNase treatment (Ingolia et al., 2009), in *Arabidopsis* seedlings. Our data represented a 3-nucleotide periodicity along the ORF, a hallmark of translation elongation (Figure S1A). We combined this high-resolution ribosome profiling and the miRNA target prediction (Dai et al., 2018) to identify the ribosome-stalling position upstream of the predicted miRNA binding sites (Table S1). Along with earlier studies

(Hou et al., 2016; Li et al., 2016; Bazin et al., 2017), our ribosome profiling has shown that specific miRNAs, including miR390 and miR173, can induce ribosome stalling 12–13 nucleotide upstream of their binding sites in *Arabidopsis thaliana* Figure 1A–C and S1B–D). These particular miRNAs are known to trigger the production of phased secondary small interfering RNAs (siRNAs), called trans-acting siRNAs (tasiRNAs), from precursors called TAS RNAs (Liu et al., 2020). tasiRNA production requires various factors including AGO7 and AGO1, which form specific RISCs with miR390 and miR173, respectively (Montgomery et al., 2008; Endo et al., 2013; Liu et al., 2020). One important factor for tasiRNA biogenesis is SUPPRESSOR OF GENE SILENCING 3 (SGS3) (Mourrain et al., 2000; Peragine et al., 2004; Vazquez et al., 2004; Allen et al., 2005). Given that SGS3 forms cytoplasmic foci named "siRNA bodies" with AGO7 (Jouannet et al., 2012) and interacts with AGO1 associating with miR173 and other 22-nt small RNAs (Chen et al., 2010; Cuperus et al., 2010; Yoshikawa et al., 2013), we reasoned that SGS3 influences miRNA-mediated ribosome stalling. To test this idea, we examined the impact of an SGS3 mutation on miRNA-mediated ribosome stalling by comparing ribosome profiling in wild-type and *sgs3-11 Arabidopsis* seedlings (Peragine et al., 2004). We observed dramatic decreases in ribosome stalling in *sgs3-11* mutants (Figure 1B and C and S1B–D and S2). This reduction cannot be explained by a change in mRNA or miRNA abundance in the mutant (Figure 1B and C and S1–3). Thus, we concluded that SGS3 is required for ribosome stalling by miR390 and miR173. Given that *sgs3-11* mutation did not cause an overall decrease in ribosome occupancy (Figure

S2), SGS3 is not a general ribosome stalling factor, but rather a specific stalling enhancer for miRNA-mediated ribosome stalling.

SGS3 and RISC cooperatively stall ribosomes *in vitro*

Although our ribosome profiling data demonstrate the involvement of SGS3 and miRNAs in ribosome stalling, how these factors coordinately pause ribosomes was unclear. To reveal the mechanisms of miRNA- and SGS3-dependent ribosome stalling, we adopted a tobacco BY-2 cell-free system, which can recapitulate miRNA-mediated RNA silencing *in vitro* (Figure 2A) (Iki et al., 2010; Iwakawa and Tomari, 2013). We used TAS3a as a representative target RNA. TAS3a contains a short (51 codon) ORF and two miR390-binding sites: one is adjacent to the stop codon and immediately downstream of the ribosome stalling site, and the other is located well downstream of those elements (Figure 2B) (Axtell et al., 2006). Ribosome stalling within the short ORF was monitored by detecting peptidyl-tRNAs, a hallmark of ribosome stalling (Nakatogawa and Ito, 2001; Muto et al., 2006), by western blotting to a FLAG-tag inserted in the F-TAS3 ORF (Figure 2A and C). Western blotting followed a neutral pH gel electrophoresis that prevents hydrolysis of the ester linkage between the tRNA and amino acid (Nakatogawa and Ito, 2001), thus enabling us to detect peptidyl-tRNAs within stalled ribosomes through an ~18 kDa upshift —the size of the tRNA moiety (Figure 2C). Translation of the reporter (F-TAS3) in the presence of AGO7-RISC led to a clear band-shift (Figure 2D and E). Disappearance of this signal after RNase treatment confirmed that the upshifted band corresponds to peptidyl-tRNA (Figure 2D).

The two miR390-binding sites in TAS3a are functionally distinct; the 5′ possesses central mismatches that preclude RISC-mediated target cleavage but allow stable binding, whereas the 3′ miR390 binding site is centrally matched with the miR390 and thus cleaves the TAS3a RNA (Figure 2B) (Axtell et al., 2006). The adjacent 5′ binding site is essential for ribosome stalling. Mutations in the critical region for miRNA recognition of the 3′ miR390 binding site (Figure 2B, F-TAS3_3M) did not impair ribosome stalling, whereas also mutating the 5′ binding site (Figure 2B, F-TAS3_5M_3M) reduced stalling (Figure 2D and E). Thus, ribosome stalling requires base-pairing between miR390 in AGO7-RISC and the 5′ miR390-binding site in TAS3a. As the 3′ site mutation increased peptidyl-tRNA accumulation, presumably by stabilizing the mRNA since it is no longer cleaved (Figure 2D), we decided to use F-TAS3_3M for further experiments.

We next sought to investigate the impact of SGS3 on ribosome stalling. Because endogenous SGS3 (NtSGS3) is abundant in BY-2 cells (Yoshikawa et al., 2013), we immuno-depleted NtSGS3 from the lysate (Figure 2F) and found decreased ribosome stalling (Figure 2G and H). Supplementing with recombinant AtSGS3 markedly rescued ribosome stalling efficiency (Figure 2F–H), indicating that SGS3 is a critical and limiting factor for miRNA-mediated ribosome stalling. Taken altogether, our *in vitro* system faithfully recapitulated ribosome stalling triggered by AGO7-RISC and SGS3.

SGS3 binding to the 3′ end of initiator microRNAs is required for ribosome pausing

146 The functional roles of AGO7-RISC and SGS3 prompted us to hypothesize that these two
147 factors form a complex that promotes ribosome stalling. SGS3 is an RNA-binding protein
148 that preferentially binds RNA duplexes with a 5′ overhang (Fukunaga and Doudna, 2009).
149 In theory, such a substrate is formed between the 3′ end of miR390 within AGO7 and the
150 5′ end of the miR390-binding site. We therefore hypothesized that SGS3 directly interacts
151 with the end of the dsRNA protruding from AGO7. To test this scenario, we first examined
152 the interaction between SGS3 and AGO7-RISC. The FLAG-tagged AGO7 mRNA was
153 translated in the BY-2 cell lysate, then the miR390 duplex was added to program RISC.
154 After further incubation with TAS3 mRNAs, the reaction mixture was used for co-
155 immunoprecipitation with anti-FLAG antibody (Figure 3A). This assay revealed that
156 endogenous NtSGS3 binds AGO7-RISC only in the presence of both miR390 and TAS3
157 variants with a wild-type 5′ site (Figure S4A). Remarkably, introducing mismatches at
158 the 5′ end of the miR390-binding site (Figure 3B, TAS3_5endM_3M) or using a miR390
159 variant that is one-nucleotide shorter (20 nt) (Figure 3B), which is not predicted to
160 protrude from AGO7, disrupted the interaction between NtSGS3 and AGO7-RISC
161 (Figure 3B–D, Figure S4B). These results strongly support a model where SGS3 forms a
162 complex with AGO7-RISC via dsRNA with a 5′ overhang formed at the 3′ end of miR390.
163 To test whether SGS3 directly interacts with the 3′ end of miR390 on the *TAS3*
164 RNA, we performed a site-specific UV crosslinking assay, in which molecules
165 neighboring the 3′ end of miR390 can be captured. We first substituted the 3′ end cytidine
166 of miR390 with a photo-reactive 4-thiouridine (Figure S4C, miR390_4SU), and restored
167 base-pairing using a TAS3a variant with a G-to-A substitution at the 5′ miR390 binding

site (Figure S4C, G21A substitution). This variant successfully rescued the interaction between miR390_21_4SU-loaded AGO7 and NtSGS3 (Figure S4C and D). In this context of the reporter, proteins crosslinked to 5′ radiolabeled miR390_21_4SU were separated on an SDS-PAGE gel (Figure 3E). In the absence of the target RNA, a specific band appeared at around 120 kDa (Figure 3F, red arrowhead). Immunoprecipitation using the anti-FLAG antibody revealed that the band corresponds to F-AGO7 (Figure 3G, red arrowheads). Strikingly, addition of the target RNA changed the crosslinked protein from AGO7 to a ~90 kDa protein (Figure 3F). This protein was immunoprecipitated with anti-NtSGS3 antibody (Figure 3H, Beads), and specifically depleted from the supernatant of the lysate after immunoprecipitation (Figure 3H, Sup), corroborating the identity of this ~90 kDa crosslinked protein as NtSGS3. These results indicate that target binding alters protein interactions at the 3′ end of miR390, switching them from AGO7 to SGS3, likely via conformational changes in AGO7-RISC.

To test if the physical interaction between SGS3 and AGO7-RISC is critical for ribosome pausing, we performed *in vitro* ribosome stalling experiments under conditions where SGS3 fails to bind AGO7-RISC using reporter variant F-TAS3_5endM_3M or the short 20-nt version of miR390. In both cases, stalling efficiencies were significantly decreased (Figure 3I–L). Taken together, we find a direct interaction between SGS3 and the 3′ end of 21-nt miR390 bound to AGO7-RISC is necessary for ribosome stalling on TAS3 mRNA.

It is worth noting that the required length of miRNA for SGS3 binding and ribosome pausing may differ between partner AGO proteins. In contrast to AGO7,

AGO1—bound by most miRNAs—requires a 22-nt long miR173 for both SGS3 interaction and ribosome stalling (Figure 4A–D) (Yoshikawa et al., 2013). As miRNAs are typically 21-nt long, plants may have evolved a AGO1 structure that fully encapsulates the 21-nt miRNAs, thus limiting promiscuous SGS3 binding and ribosome stalling (Figure 4C and D). Importantly, we find that ribosome pausing occurs even if TAS1 is cleaved by AGO1-RISC loaded with 22-nt miR173 (Figure 4D and E). This is not limited to the TAS1 and miR173-AGO1 pair. AGO7-miR390-SGS3 complex also stalls ribosomes on the cleavable binding site which has perfect complementarity to miR390 (Figure S5A–C). Because AGO-miRNA-SGS3 complex holds and stabilizes both 5′ and 3′ RNA fragments after target cleavage (Figure 4E) (Yoshikawa et al., 2013), we reasoned that SGS3 and RISC can stay on the cleaved targets long enough to stall ribosomes.

Ribosome stalling is not an essential event but a positive modulator for the production of secondary siRNAs

The striking correspondence between ribosome stalling and TAS precursors (Figure 1 and S1B–D) led us to hypothesize that ribosome pausing by the SGS3-miRNA complex promotes tasiRNA production. So far, several studies have focused on the relationship between translation and tasiRNA biogenesis (Zhang et al., 2012; Hou et al., 2016; Li et al., 2016; Yoshikawa et al., 2016; Bazin et al., 2017). However, it is still controversial if positioning of the miRNA-binding site in the CDS or near the stop codon is important for tasiRNA production (Zhang et al., 2012; Yoshikawa et al., 2016; Bazin et al., 2017). For

example, previous quantitative RT-PCR (qRT-PCR) experiments showed no significant changes in tasiRNA production between the wild-type TAS3 and a mutant TAS3 that possesses an early stop codon located far upstream of the 5′ miR390 binding site (Bazin et al., 2017), suggesting that ribosome stalling has no impact on the tasiRNA biogenesis. To carefully assess the impact of ribosome stalling on tasiRNA biogenesis, we first attempted to construct TAS3 variants with no ribosome stalling that retain binding to AGO7 and SGS3. Such variants were obtained by inserting 4 or more nucleotides between the stop codon and 5′ miR390 binding site in TAS3 (Figure 5A and B, S6). As ribosomes stall one-codon upstream of the stop codon in TAS3, we reasoned that these insertions promote normal translation termination without interfering in the binding between AGO7-RISC and SGS3.

To test the hypothesis that ribosome pausing promotes the production of tasiRNAs, we compared tasiRNA accumulation in different TAS3 variants in *Nicotiana benthamiana* leaves. We opted to use Northern blotting for accurate detection of the secondary siRNAs, because this method can distinguish the canonical secondary siRNAs from the non-specific RNA fragments derived from the TAS3 reporters by size. Co-expression of miR390 and AGO7 efficiently produced 21-nt tasiRNAs, compared with the 5′ miR390 binding site mutant (TAS3_5M) (Figure 5C–E). Thus, our transient assay successfully recapitulated canonical TAS3 tasiRNA biogenesis. Importantly, placing the 5′ miR390 binding site 6-nucleotide away (Figure 5C, TAS3+6) significantly reduced tasiRNA production to ~60% (Figure 5D and E), suggesting that clearance of stalled ribosomes impairs efficient tasiRNA production. In contrast, tasiRNA production from a

TAS3 variant with a 3-nucleotide insertion (Figure 5C, TAS+3), which still stalls ribosomes, was comparable to that from wild-type TAS3 (Figure 5D and E). To confirm if ribosome stalling enhances the tasiRNA biogenesis, we introduced artificial tandem stop codons at the ~120 nt upstream of the miR390 target site (early_stop), which forces ribosomes to terminate without stalling (Figure 5C). In contrast to the previous report (Bazin et al., 2017), our quantitative Northern blotting revealed that the tandem early stop codons significantly reduced tasiRNA production to ~60%, similarly to TAS3+6 (Figure 5D and E). These data were not explained by changes in precursor *TAS3* abundance (Figure 5F and G). Altogether, we conclude that ribosome stalling regulates secondary siRNA production in a manner different from stabilization of mRNAs.

Discussion

Here, we find that the dsRNA-binding protein SGS3 forms ribosome stalling complexes on the protruding end of the dsRNA formed between the TAS RNAs and miR390-AGO7 or 22-nt miR173-AGO1-RISC (Figure 6). In general, the ribosome displaces RNA binding proteins bound to mRNAs during elongation (Halstead et al., 2016), suggesting that SGS3 imposes an extreme barrier for trailing ribosomes. A recent study suggested that unconventional base-pairing between human miRNAs and target sites cause transient ribosome stalling (Zhang et al., 2018). Although the precise stalling mechanism remains unclear in animals, there may be an RNA-binding protein(s) that protects the 3′ end of miRNA from the helicase activity of ribosomes.

The accumulating evidence suggests that translation alters the biogenesis of TAS3 tasiRNAs (Li et al., 2016; Bazin et al., 2017). A previous study showed that the position of the start site is critical for the stability of TAS3 mRNAs and tasiRNA biogenesis (Bazin et al., 2017). We here demonstrate that ribosome stalling enhances TAS3 tasiRNA biogenesis (Figure 5D, E and 6). This is supported from an evolutionary standpoint; many plant species have the 5′ miR390 binding site just downstream the stop codon or in the CDS of TAS3 (Table S2). This positive effect of ribosome pausing for secondary siRNA production may not be limited to TAS3 genes. It was previously shown that a miR173 binding site located within ORF also enhances secondary siRNA biogenesis (Zhang et al., 2012; Yoshikawa et al., 2016), suggesting that ribosome stalling promotes tasiRNA biogenesis on TAS1/2 genes and other 22-nt miRNA target genes. On the other hand, ribosome stalling is not a prerequisite for triggering secondary siRNA biogenesis. Indeed, TAS3+6 and early_stop still produced tasiRNAs in our transient assays with *Nicotiana benthamiana* plants (Figure 5D and E). Thus, although stalled ribosomes positively regulate tasiRNA production, SGS3-miRNA-AGO complex can trigger tasiRNAs independently of translational arrest (Figure 6). The molecular details of how ribosome stalling enhances tasiRNA production warrant future studies. Given that arrest peptide-mediated ribosome-pausing induces changes in mRNA localization in animal cells (Yanagitani et al., 2011), we suggest that miRNA-mediated ribosome pausing may facilitate the delivery of the tasiRNA precursors to a secondary siRNA “factory”, such as the siRNA body (Jouannet et al., 2012).

We observed SGS3- and RISC-dependent ribosome stalling in five TAS loci in *Arabidopsis* (Figure 1). However, they may be just a tip of the iceberg of miRNA-mediated ribosome pausing. There are many DNA regions named PHAS loci that produce phased secondary siRNAs (phasiRNAs) by the same mechanism as TAS loci (Liu et al., 2020). Although our ribosome profiling failed to detect obvious ribosome stalling 11–14 nt upstream of miRNA binding sites in known PHAS loci (Figure 1 and Table S1), more sensitive methods like single-molecule imaging (Ruijtenberg et al., 2020) may reveal ribosome stalling on the miRNA-bound targets. In addition to miRNAs, siRNAs may also induce ribosome stalling. A recent study demonstrates that 22-nt siRNAs, which have the potential to recruit SGS3, accumulate upon environmental stress, trigger the RNA silencing amplification, and mediate translational repression (Wu et al., 2020). Such 22-nt siRNAs are also induced by viral infection (Mourrain et al., 2000; Akbergenov et al., 2006; Deleris et al., 2006; Diaz-Pendon et al., 2007; Garcia-Ruiz et al., 2010). Therefore, SGS3- and miRNA/siRNA-mediated ribosome stalling is likely to have an impact on a wider range of cellular processes such as stress adaptation and antiviral immunity in plants.

Methods

General methods.

Preparation of tobacco BY-2 lysate, substrate mixture (containing ATP, ATP-regeneration system, and amino acid mixture), 1×lysis buffer [30 mM HEPES-KOH (pH 7.4), 100 mM potassium acetate, 2 mM magnesium acetate], and microRNA duplexes (Table S3) have been previously described in detail (Tomari and Iwakawa, 2017). mRNAs were transcribed *in vitro* from NotI- (for plasmids with the prefix "pBYL-") or XhoI- (for plasmids with the prefix "pUC57-") digested plasmids or PCR products using the AmpliScribe T7 High Yield Transcription Kit (Lucigen), followed by capping with ScriptCap m^7G Capping System (Cell Script). Poly(A)-tails were added to transcripts from pUC57-plasmids or PCR products using the T7 promoter by A-Plus Poly(A) Polymerase Tailing Kit (Cell Script). Anti-AtSGS3 (diluted at 1:3000) and anti-AtAGO7 antibodies (diluted at 1:3000) were raised in rabbits using synthetic peptides (NH_2-MSSRAGPMSKEKNVQGGC-COOH) and (NH_2-IPSSKSRTPLLHKPYHHC-COOH) as antigens respectively, and affinity-purified (Medical & Biological Laboratories).

Plants and growth conditions.

Arabidopsis thaliana wild-type (Col-0) and the *sgs3-11* mutant (Peragine et al., 2004) were used in this study. Seeds were incubated in 70% EtOH at room temperature for 2 min, sterilized with liquid sodium hypochlorite, washed 5 times in sterile water, sown on filter paper (Whatman No.2), laid on Murashige and Skoog (MS)-agar plates (1×MS salt,

315 1% sucrose, 1% agar, pH 5.7) and incubated at 4°C for 3 days. After vernalization, the
316 plates were incubated at 22°C for 3 days under continuous LED light (LC-LED450W,
317 TAITEC).
318
319 **Ribosome profiling.**
320 Briefly, 0.2 g of frozen seedlings and 400 µl of *Arabidopsis* lysis buffer (100 mM Tris-
321 HCl pH 7.5, 40 mM KCl, 20 mM $MgCl_2$, 1 mM DTT, 100 µg/ml cycloheximide and 1%
322 Triton X-100) were crushed into a powder using the Multi-beads shocker (Yasui Kikai).
323 The 3000 × g supernatant of the lysate was mixed with 25 µl of Turbo DNase (Thermo
324 Fisher Scientific) and incubated on ice for 10 min. RNA concentration was measured with
325 a Qubit RNA BR Assay Kit (Thermo Fisher Scientific). Ribosome footprints ranging
326 between 17 and 34 nt were gel-purified and subsequent library preparation were executed
327 as previously described (McGlincy and Ingolia, 2017; Kurihara et al., 2018). Two
328 libraries from two biological replicates (WT_rep1, WT_rep2, sgs3_rep1 and sgs3_rep2)
329 were sequenced on a HiSeq4000 (Illumina). 24 to 29 nt footprints were mapped onto the
330 TAIR10 *Arabidopsis thaliana* genome sequence, excluding rRNA/tRNAs. Empirically,
331 A-site position was estimated as 11 for 24 nt, 12 for 25 nt, 13 for 26 nt, 14 for 27 nt, 15
332 for 28 nt, 16 for 29 nt, based on the homogeneous 5′ end of the reads. The relative
333 ribosome occupancy r at position j in an ORF of gene g of length l is defined as follows:
334
335 $$r_{gj} = \frac{f_{gj}}{d_{gj}}$$

where

$$d_{gj} = \frac{\left(\sum_{i=1}^{l} f_i\right) - f_j}{l - 1}$$

f_{gj} is the footprint at position j in a ORF of gene g. r_{gj} is a ratio of f_{gj} to the average footprint across nucleotide positions on the ORF of the same gene, d_{gj}.

microRNA target prediction.

The targets of mature *Arabidopsis* microRNA sequences [miRbase (miRbase20) (Kozomara and Griffiths-Jones, 2011; Kozomara and Griffiths-Jones, 2014)] were predicted using the psRNATarget server (Dai and Zhao, 2011; Dai et al., 2018) with the following settings: # of top targets = 15, Expectation = 3, Seed region = 2-8 nt.

RNA-seq.

Total RNA was extracted from seedlings with Trizol (Thermo Fisher Scientific). Library construction and deep sequencing were performed by AnnoRoad in Beijing. Reads were mapped to the transcripts of *Arabidopsis thaliana* (derived from TAIR10, ver. 10 released on 2010 in psRNATarget server (Dai and Zhao, 2011; Dai et al., 2018)) by Bowtie2(Langmead and Salzberg, 2012). Sam files were converted to bam files using SAMtools (Li et al., 2009) and then to bed files with BEDTools (Quinlan and Hall, 2010). BEDtools (Quinlan and Hall, 2010) was used to calculate the depth of coverage for every base across mRNAs shown in Figure 1B, C, S1B–D.

Plasmid construction.

The following constructs used in this study have been previously described: pBYL2 (Mine et al., 2010), pBYL-AGO1 (Endo et al., 2013), pBYL-AGO7 (Endo et al., 2013), pBYL-3×FLAG-AGO7 (Endo et al., 2013), pBYL-3×FLAG-AGO1 (Endo et al., 2013), pBYL-3×FLAG-SUMO-AtAGO1 (Iwakawa and Tomari, 2013), pAT006 (Tsuzuki et al., 2014), pMDC32 (Curtis and Grossniklaus, 2003), pMDC-Tas3a (Montgomery et al., 2008), pMDC-HA-AGO7 (Montgomery et al., 2008), pMDC-miR390 (Montgomery et al., 2008). The DNA fragments used for plasmid construction are listed in Table S4.

pBYL-3×HA

A DNA fragment containing the T7 promoter, 5′ UTR of *Arabidopsis thaliana* alcohol dehydrogenase 1 and 3×HA tag (T7_ADH_5UTR_*3×HA,* Table S4) was cloned into XbaI/AscI-digested pBYL2 vector using the HiFi DNA Assembly Cloning kit (New England Biolabs).

pBYL-3×HA-AGO7

A DNA fragment containing AGO7 ORF was amplified by PCR with pBYL-AGO7(Endo et al., 2013) using primers oligoE1 and oligoE2, digested by AscI, and cloned into AscI-digested pBYL-3×HA vector by ligation.

pBYL-3×HA-AGO1

A PCR fragment with AGO1 ORF following 3×HA tag was amplified by overlap

379 extension PCR with pBYL-AGO1 (Endo et al., 2013) as template using primers
380 oligo1118 and oligo1094. The fragment was cloned into AscI-digested pBYL2 vector via
381 HiFi DNA Assembly Cloning kit (New England Biolabs).
382
383 *pUC57-TAS3*
384 The TAS3a sequence (AT3G17185.1) following T7 promoter (T7_TAS3a, Table S4) was
385 inserted into EcoRV-digested pUC57 vector via GenScript gene synthesis service.
386
387 *pUC57-F-TAS3*
388 Three DNA fragments were prepared by PCR: TAS3a_5′ UTR fragment amplified from
389 pUC57-TAS3 using primers oligo1062 and oligo1063, 3×FLAG tag sequence amplified
390 using two oligos, oligo1064 and oligo512 and the TAS3a ORF amplified from pUC57-
391 TAS3 using primers, oligo1065 and oligo1066. The three DNA fragments were cloned
392 into SacII/XhoI-digested pUC57-TAS3a via HiFi DNA Assembly Cloning kit (New
393 England Biolabs).
394
395 *pUC57-F-TAS3_3M*
396 Seven nucleotide mismatches were introduced into the 3′ miR390 binding site (Figure
397 2C) in pUC57-F-TAS3 by site directed mutagenesis using primers oligo1073 and
398 oligo1074.
399
400 *pUC57-F-TAS3_5M_3M*

Seven nucleotide mismatches were introduced into the 5′ miR390 binding site (Figure 2C) in pUC57-F-TAS3_3M by site directed mutagenesis using primers oligo 1099 and oligo1100.

pUC57-F-TAS3_3M(+1), pUC57-F-TAS3_3M(+2), pUC57-F-TAS3_3M(+3), pUC57-F-TAS3_3M(+4), pUC57-F-TAS3_3M(+5), pUC57-F-TAS3_3M(+6) and pUC57-F-TAS3_3M(+7)

One to six nucleotides, as shown in Figure 5A, were inserted between the stop codon of the short ORF and 5′ miR390 binding site in pUC57-F-TAS3_3M by site directed PCR using primer pairs of oligo1180-oligo1181, oligo1182-oligo1183, oligo1161-oligo1162, oligo1163-oligo1164, oligo1165-oligo1166, oligo1167-oligo1168 and oligo1169-oligo1170, respectively.

pEU-6×His-SBP-SUMO-AtSGS3

Two DNA fragments were prepared by PCR: 6×His-SBP-SUMOstar-tag fragment amplified from pASW-SUMO-AtRDR6 (Opt) (Baeg et al., 2017) using oligo1044 and oligo1039 and SGS ORF fragment amplified from cDNA of *Arabidopsis thaliana* using oligoK1 and oligoK2. The two DNA fragments were inserted into EcoRV/SmaI-digested pEU-E01-MCS vector via HiFi DNA Assembly Cloning kit (New England Biolabs).

pBYL-3×FLAG-SUMOstar-tag-AGO7

Two PCR products were prepared by PCR: 3×FLAG-SUMOstar-tag fragment amplified

423 from pBYL-3×FLAG-SUMO-AtAGO1 (Iwakawa and Tomari, 2013) using primers
424 oligo955 and oligo1039 and AGO7 fragment amplified from pBYL-AGO7 (Endo et al.,
425 2013) using primers oligo1159 and oligo1160. The two fragments were cloned into AscI-
426 digested pBYL2 vector (Mine et al., 2010) via HiFi DNA Assembly Cloning kit (New
427 England Biolabs).
428
429 *pUC57-F-TAS3_5endM_3M and pUC57-F-TAS3_5P_3M*
430 The 5′ miR390-binding site in pUC57-F-TAS3_3M was replaced by the sequences shown
431 in Figure 3B and Figure S5 by site directed mutagenesis using primer pairs oligo1101-
432 oligo1102 and oligo 1106-oligo1107, respectively.
433
434 *pUC57-TAS3_3M, pUC57-TAS3_5endM_3M, pUC57-TAS3_5P_3M, pUC57-*
435 *TAS3_M(+1), pUC57-TAS3_M(+2), pUC57-TAS3_M(+3), pUC57-TAS3_M(+4),*
436 *pUC57-TAS3_M(+5), pUC57-TAS3_M(+6) and pUC57-TAS3_M(+7)*
437 The 3×FLAG tag sequences were removed from the corresponding pUC57-F-TAS3
438 constructs shown above by site directed mutagenesis using primers oligo1197 and
439 oligo1198.
440
441 *pUC57-TAS3_G21A_3M*
442 The 5′ terminal G nucleotide of 5′ miR390-binding site in pUC57-TAS3_3M was
443 substituted to A by site directed mutagenesis using primers oligo1220 and oligo1221.
444

pCR-Blunt II-TOPO_TAS1a

TAS1a PCR product was amplified from cDNA corresponding to *Arabidopsis* seedling total RNA using oligoA1 and oligoA2 for the TAS1a sequence and cloned into pCR Blunt II-TOPO vector (Invitrogen, #45-0245).

pCR-Blunt II-TOPO_3×FLAG-TAS1a

Three PCR fragments were prepared from pCR-Blunt II-TOPO_TAS1a: TOPO-TAS1a 5′ UTR fragment amplified with oligoA3 and oligoA4, FLAG-TAS1a fragment amplified with oligoA5 and oligoA6 and ORF-3′ UTR-TOPO fragment amplified with oligoA7 and oligoA8. To insert the 3×FLAG sequence directly in front of ORF1, the above three PCR fragments were cloned into XhoI/SpeI-digested pCR Blunt II-TOPO vector (Invitrogen) using the HiFi DNA Assembly Cloning kit (New England Biolabs).

T7-TAS1a and T7-F-Tas1a

T7-TAS1a and T7-F-Tas1a DNA templates were amplified from pCR-Blunt II-TOPO_TAS1a and pCR Blunt II-TOPO-3xFLAG-TAS1a, respectively, using a forward primer containing T7 polymerase binding site (oligoA9) and a reverse primer with poly(A) tail (oligoA10).

pAT006-TAS3a-PDS_full-length

A TAS3a fragments with a full-length 5′ UTR, a natural intron and tandem synthetic-tasiRNAs in the 5′ D7[+] and 5′ D8[+] positions (TAS3aPDS2) was synthesized via

GeneArt Strings DNA Fragments service (invitrogen), gel-purified and cloned into SalI/SpeI-digested pAT006 (Tsuzuki et al., 2014) vector via HiFi DNA Assembly Cloning kit (New England Biolabs).

pMDC32_TAS3

Two PCR products were amplified: fragment A from pAT006-TAS3a-PDS_full-length using primers oligo1201 and oligo1202 and fragment B from pMDC-Tas3a (Montgomery et al., 2008) using primers oligo1203 and oligo1204. The two fragments were cloned into KpnI/SpeI-digested pMDC32 vector via HiFi DNA Assembly Cloning kit (New England Biolabs).

pMDC32_TAS3_5M

Two PCR products were amplified: fragment A from pAT006-TAS3a-PDS_full-length using primers oligo1201 and oligo1209 and fragment B from pMDC-Tas3a (Montgomery et al., 2008) using primers oligo1210 and oligo1204. The two fragments were cloned into KpnI/SpeI-digested pMDC32 vector via HiFi DNA Assembly Cloning kit (New England Biolabs).

pMDC32_early_stop

Two PCR products were amplified: fragment A from pAT006-TAS3a-PDS_full-length using primers oligo1201 and oligo1211 and fragment B from pMDC-Tas3a (Montgomery et al., 2008) using primers oligo1212 and oligo1204. The two fragments were cloned into

KpnI/SpeI-digested pMDC32 vector via HiFi DNA Assembly Cloning kit (New England Biolabs).

pMDC32_TAS3(+3)

Two PCR products were amplified: fragment A from pAT006-TAS3a-PDS_full-length using primers oligo1201 and oligo1207 and fragment B from pMDC-Tas3a (Montgomery et al., 2008) using primers oligo1208 and oligo1204. The two fragments were cloned into KpnI/SpeI-digested pMDC32 vector via HiFi DNA Assembly Cloning kit (New England Biolabs).

pMDC32_TAS3(+6)

Two PCR products were amplified: fragment A from pAT006-TAS3a-PDS_full-length using primers oligo1201 and oligo1205 and fragment B from pMDC-Tas3a (Montgomery et al., 2008) using primers oligo1206 and oligo1204. The two fragments were cloned into KpnI/SpeI-digested pMDC32 vector via HiFi DNA Assembly Cloning kit (New England Biolabs).

Production of recombinant AtSGS3 protein

Recombinant AtSGS3 proteins were expressed using the Premium PLUS Expression kit (Cell-Free Sciences) with pEU-6×His-SBP-SUMO-AtSGS3 according to manufacturer instructions. The protein was affinity purified with streptavidin sepharose high performance beads (GE Healthcare), washed three times with l × lysis buffer containing

200 mM NaCl and 0.1% TritonX-100, rinsed once with 1 × lysis buffer containing 20% glycerol and 1mM DTT and eluted by 1 × lysis buffer containing 20% glycerol, 1 mM DTT and 0.05 U/µl of SUMOstar protease. Protein concentration was determined using SDS-PAGE with defined dilutions of BSA as concentration standards.

In vitro RNA silencing assay, NuPAGE and Western blotting

Typically, 7.5 µl of BY-2 lysate, 3.75 µl of substrate mixture, and 0.75 µl of 300 nM AGO mRNAs were mixed and incubated at 25°C for 30 min. To assemble RISC, 1.5 µl of 1.5 µM miR390 or miR173 duplex was added to the reaction mixture and incubated at 25°C for 90 min. Then, 1.5 µl of 100 nM TAS3a or TAS1a variant was added and further incubated at 25°C for 10–60 min. For RNase treatment, 5 µl of the reaction was treated with 1 µl of RNase mixture (10% RNase A, Sigma + 20% RNase One, Promega), incubated at 37°C for 10 min and then mixed with 6 µl of 2 × SDS-PAGE buffer. For the control, 1 µl sterile water was used instead of RNase mixture. The samples were run on NuPAGE Bis-Tris Precast Gel (Thermo Fisher Scientific) at 200 V for ~30 min in 1 × NuPAGE MES SDS Buffer (Thermo Fisher Scientific) and transferred onto PVDF membrane. Western blotting was performed as previously described (Tomari and Iwakawa, 2017) with modifications. The membrane was blocked in TBST containing 1.0% nonfat dried milk (w/v) for 30 min. Anti-AtSGS3 (diluted at 1:3000), anti-AtAGO7 antibodies (diluted at 1:3000), anti-NtSGS3 antibody (diluted at 1:3000) (Yoshikawa et al., 2013), anti-DDDDK-tag mAb (diluted at 1:5000) (Medical & Biological Laboratories) and anti-HA-tag mAb (diluted at 1:5000) (Medical & Biological

Laboratories) were used as primary antibodies. Peroxidase AffiniPure Goat Anti-Rabbit IgG (H+L) (diluted at 1:20000) (Jackson ImmunoResearch), Anti-IgG (H+L) (Mouse) pAb-HRP (diluted at 1:5000) (Medical & Biological Laboratories) and Mouse TrueBlot ULTRA: Anti-Mouse Ig HRP (Rockland Immunochemicals, Inc.) (1:1000) were used as secondary antibodies.

Northern blotting

For *in vitro* assays, two microliter of reaction mixture was mixed with 8 µl of low salt PK solution [0.125% SDS, 12.5 mM EDTA, 12.5 mM HEPES-KOH (pH7.4) and 12.5% Proteinase K (TaKaRa)], and incubated at 50°C for 10 min. Ten microliter of 2 × formamide dye [10 mM EDTA, pH 8.0, 98% (w/v) deionized formamide, 0.025% (w/v) xylene cyanol and 0.025% (w/v) bromophenol blue] was added into the mixture, and further incubated at 65°C for 10 minutes. For *in vivo* assays, total RNA was purified with Trizol reagent (Thermo Fisher Scientific), and 10 µl of 300–500 ng/ul total RNAs were mixed with equal volume 2 × formamide dye. Ten µl of samples were run on a denaturing 1% agarose gel, transferred to the Hybond N+ membrane with capillary blotting and fixed with UV crosslinker. For small RNAs, 10 µl of samples were run on a denaturing 18% acrylamide gel. RNAs were transferred to Hybond N membrane with electro blotting and chemically crosslinked (Pall and Hamilton, 2008). TAS3 variants were detected with Digoxigenin (DIG)-labeled long TAS3 probe (Figure 2D) or 5′ ^{32}P-radiolabeled oligo probe mixtures (oligo1230-1234) (Figure 5F). F-TAS1a and its 5′ cleaved fragment were detected with a 5′ ^{32}P-radiolabeled oligo probe (oligoA4) (Figure 4E). U6 RNA, miR173,

555 miR390, and tasiRNAs from TAS3 variants were detected with 5′ ^{32}P-radiolabeled
556 oligo1129, oligo1353, oligo1131, oligoD7, respectively.
557
558 **Immunoprecipitation with anti-FLAG antibody**
559 F-AGO7-RISC or F-AGO1-RISC was assembled as shown above. Target RNAs were
560 mixed with the RISCs at a final concentration of 50 nM, and incubated for 20 min. The
561 reaction mixture was incubated with Dynabeads protein G (Invitrogen) coated with anti-
562 FLAG antibody on a rotator at 4°C for 1 h. The beads were washed three times with 1 ×
563 lysis buffer containing 200 mM NaCl and 1% Triton-X 100 or 1 × wash buffer (20 mM
564 Hepes, pH 7.5, 120 mM KCl, 10 mM MgCl2 and 0.2% Nonidet P-40). After removing
565 buffer completely, 1×SDS-PAGE sample buffer was added to the beads. The samples
566 (input, supernatant, and beads) were heated for 5 min and used for SDS-PAGE. Western
567 blotting was performed as described above.
568
569 **Immunodepletion of endogenous SGS3 protein**
570 Fifty microliter of BY-2 lysate was mixed with 1.66 µg of anti-NtSGS3 (Yoshikawa et al.,
571 2013) or Normal Rabbit IgG (Medical & Biological Laboratories) at 4°C for 1h. To
572 remove the antibodies and binding proteins thereof, the lysate was mixed with the pellet
573 of 50 µl Dynabeads protein G, and incubated at 4°C for 1h. The supernatant was
574 transferred into new tubes. After flash freezing by liquid nitrogen, the SGS3 or Mock-
575 depleted lysate was stored at -80°C .
576

577 **Photoactivated UV crosslinking**

578 *In vitro* reaction mixtures were prepared as outlined above (*Immunoprecipitation with*
579 *anti-FLAG antibody*) with F-AGO7, ^{32}P-labeled miR390_21_4SU, and TAS3-G21A-3M.
580 The sample was transferred to Terasaki plate wells (7 µl/well) and exposed to > 300 nm
581 UV radiation for 15 s using a UV crosslinker (SP-11 SPOT CURE, USHIO) with a
582 uniform radiation lens (USHIO) and a long-path filter (300 nm, ASAHI SPECTRA) at 3
583 cm from the light. For input sample, aliquots of reaction mixture were transferred into a
584 new tube, and mixed with 4×SDS-PAGE sample buffer. For FLAG-IP, the reaction
585 mixture was incubated with Dynabeads protein G coated with anti-FLAG antibody on a
586 rotator at 4°C for 1 h. For SGS3-IP, the reaction mixture was first incubated with anti-
587 NtSGS3 antibody at 4°C for 1 h, then with Dynabeads protein G at 4°C for another 1 h.
588 The tube was then placed on a magnetic stand to transfer the supernatant into a new tube,
589 which was then mixed with 4×SDS-PAGE sample buffer. The beads were washed three
590 times with 1×lysis buffer containing 800 mM NaCl and 1% Triton-X 100. After removing
591 the buffer completely, 1×SDS-PAGE sample buffer was added to the beads. The samples
592 (input, supernatant, and beads) were heated for 5 min and used for SDS-PAGE. After
593 drying, the gel was exposed to a phosphor imaging plate.
594
595 **Agrobacterium-based transient expression in *Nicotiana benthamiana***
596 The *Nicotiana benthamiana* infiltration assay was performed as previously described
597 (Llave et al., 2000). Briefly, pAT006 and pMDC- plasmids were introduced into
598 *Agrobacterium tumefaciens* GV3101 (pMP90). The *Agrobacterium* cells transformed

599 with TAS3 constructs, AGO7, and miR390 or empty vector (pAT006) were pooled at a
600 ratio of 1:1:2 (total optical density at 600 nm (OD600)) = 1.0). The leaves were harvested
601 at ~48 h post-infiltration. Total RNA was extracted using Trizol reagent (Thermo Fisher
602 Scientific).
603

604 **Data availability**

605 All sequencing data are publicly available in DDBJ, under the accession number
606 DRA010034 (currently undisclosed). All other data are available from the authors upon
607 reasonable request.
608

609 **References**

610 Akbergenov, R., Si-Ammour, A., Blevins, T., Amin, I., Kutter, C., Vanderschuren, H.,
611 Zhang, P., Gruissem, W., Meins, F., Hohn, T., and Pooggin, M. M. (2006). Molecular
612 characterization of geminivirus-derived small RNAs in different plant species. Nucleic
613 Acids Res *34*, 462-471.
614 Allen, E., Xie, Z., Gustafson, A. M., and Carrington, J. C. (2005). microRNA-directed
615 phasing during trans-acting siRNA biogenesis in plants. Cell *121*, 207-221.
616 Axtell, M. J., Jan, C., Rajagopalan, R., and Bartel, D. P. (2006). A two-hit trigger for
617 siRNA biogenesis in plants. Cell *127*, 565-577.
618 Baeg, K., Iwakawa, H. O., and Tomari, Y. (2017). The poly(A) tail blocks RDR6 from
619 converting self mRNAs into substrates for gene silencing. Nat Plants *3*, 17036.
620 Bazin, J., Baerenfaller, K., Gosai, S. J., Gregory, B. D., Crespi, M., and Bailey-Serres,
621 J. (2017). Global analysis of ribosome-associated noncoding RNAs unveils new modes
622 of translational regulation. Proc Natl Acad Sci U S A *114*, E10018-E10027.
623 Chen, H. M., Chen, L. T., Patel, K., Li, Y. H., Baulcombe, D. C., and Wu, S. H. (2010).
624 22-Nucleotide RNAs trigger secondary siRNA biogenesis in plants. Proc Natl Acad Sci
625 U S A *107*, 15269-15274.

626 Cuperus, J. T., Carbonell, A., Fahlgren, N., Garcia-Ruiz, H., Burke, R. T., Takeda, A.,
627 Sullivan, C. M., Gilbert, S. D., Montgomery, T. A., and Carrington, J. C. (2010).
628 Unique functionality of 22-nt miRNAs in triggering RDR6-dependent siRNA
629 biogenesis from target transcripts in Arabidopsis. Nat Struct Mol Biol *17*, 997-1003.
630 Curtis, M. D., and Grossniklaus, U. (2003). A gateway cloning vector set for high-
631 throughput functional analysis of genes in planta. Plant Physiol *133*, 462-469.
632 Dai, X., and Zhao, P. X. (2011). psRNATarget: a plant small RNA target analysis
633 server. Nucleic Acids Res *39*, W155-9.
634 Dai, X., Zhuang, Z., and Zhao, P. X. (2018). psRNATarget: a plant small RNA target
635 analysis server (2017 release). Nucleic Acids Res *46*, W49-W54.
636 Deleris, A., Gallego-Bartolome, J., Bao, J., Kasschau, K. D., Carrington, J. C., and
637 Voinnet, O. (2006). Hierarchical action and inhibition of plant Dicer-like proteins in
638 antiviral defense. Science *313*, 68-71.
639 Diaz-Pendon, J. A., Li, F., Li, W. X., and Ding, S. W. (2007). Suppression of antiviral
640 silencing by cucumber mosaic virus 2b protein in Arabidopsis is associated with
641 drastically reduced accumulation of three classes of viral small interfering RNAs. Plant
642 Cell *19*, 2053-2063.
643 Endo, Y., Iwakawa, H. O., and Tomari, Y. (2013). Arabidopsis ARGONAUTE7 selects
644 miR390 through multiple checkpoints during RISC assembly. EMBO Rep *14*, 652-658.
645 Fabian, M. R., Sonenberg, N., and Filipowicz, W. (2010). Regulation of mRNA
646 translation and stability by microRNAs. Annu Rev Biochem *79*, 351-379.
647 Fukunaga, R., and Doudna, J. A. (2009). dsRNA with 5' overhangs contributes to
648 endogenous and antiviral RNA silencing pathways in plants. EMBO J *28*, 545-555.
649 Garcia-Ruiz, H., Takeda, A., Chapman, E. J., Sullivan, C. M., Fahlgren, N., Brempelis,
650 K. J., and Carrington, J. C. (2010). Arabidopsis RNA-dependent RNA polymerases and
651 dicer-like proteins in antiviral defense and small interfering RNA biogenesis during
652 Turnip Mosaic Virus infection. Plant Cell *22*, 481-496.
653 Halstead, J. M., Wilbertz, J. H., Wippich, F., Lionnet, T., Ephrussi, A., and Chao, J. A.
654 (2016). TRICK: A Single-Molecule Method for Imaging the First Round of Translation
655 in Living Cells and Animals. Methods Enzymol *572*, 123-157.
656 Hou, C. Y., Lee, W. C., Chou, H. C., Chen, A. P., Chou, S. J., and Chen, H. M. (2016).
657 Global Analysis of Truncated RNA Ends Reveals New Insights into Ribosome Stalling
658 in Plants. Plant Cell *28*, 2398-2416.

659 Iki, T., Yoshikawa, M., Nishikiori, M., Jaudal, M. C., Matsumoto-Yokoyama, E.,
660 Mitsuhara, I., Meshi, T., and Ishikawa, M. (2010). In vitro assembly of plant RNA-
661 induced silencing complexes facilitated by molecular chaperone HSP90. Mol Cell *39*,
662 282-291.
663 Inada, T. (2017). The Ribosome as a Platform for mRNA and Nascent Polypeptide
664 Quality Control. Trends Biochem Sci *42*, 5-15.
665 Ingolia, N. T., Ghaemmaghami, S., Newman, J. R., and Weissman, J. S. (2009).
666 Genome-wide analysis in vivo of translation with nucleotide resolution using ribosome
667 profiling. Science *324*, 218-223.
668 Ito, K., and Chiba, S. (2013). Arrest peptides: cis-acting modulators of translation.
669 Annu Rev Biochem *82*, 171-202.
670 Iwakawa, H. O., and Tomari, Y. (2013). Molecular Insights into microRNA-Mediated
671 Translational Repression in Plants. Mol Cell *52*, 591-601.
672 Iwakawa, H. O., and Tomari, Y. (2015). The Functions of MicroRNAs: mRNA Decay
673 and Translational Repression. Trends Cell Biol *25*, 651-665.
674 Jouannet, V., Moreno, A. B., Elmayan, T., Vaucheret, H., Crespi, M. D., and Maizel, A.
675 (2012). Cytoplasmic Arabidopsis AGO7 accumulates in membrane-associated siRNA
676 bodies and is required for ta-siRNA biogenesis. EMBO J *31*, 1704-1713.
677 Kozomara, A., and Griffiths-Jones, S. (2011). miRBase: integrating microRNA
678 annotation and deep-sequencing data. Nucleic Acids Res *39*, D152-7.
679 Kozomara, A., and Griffiths-Jones, S. (2014). miRBase: annotating high confidence
680 microRNAs using deep sequencing data. Nucleic Acids Res *42*, D68-73.
681 Kurihara, Y., Makita, Y., Kawashima, M., Fujita, T., Iwasaki, S., and Matsui, M.
682 (2018). Transcripts from downstream alternative transcription start sites evade uORF-
683 mediated inhibition of gene expression in Arabidopsis. Proc Natl Acad Sci U S A *115*,
684 7831-7836.
685 Langmead, B., and Salzberg, S. L. (2012). Fast gapped-read alignment with Bowtie 2.
686 Nat Methods *9*, 357-359.
687 Li, H., Handsaker, B., Wysoker, A., Fennell, T., Ruan, J., Homer, N., Marth, G.,
688 Abecasis, G., Durbin, R., and 1000, G. P. D. P. S. (2009). The Sequence
689 Alignment/Map format and SAMtools. Bioinformatics *25*, 2078-2079.
690 Li, S., Le, B., Ma, X., Li, S., You, C., Yu, Y., Zhang, B., Liu, L., Gao, L., Shi, T., Zhao,
691 Y., Mo, B., Cao, X., and Chen, X. (2016). Biogenesis of phased siRNAs on membrane-

692 bound polysomes in Arabidopsis. Elife *5*, e22750.
693 Liu, Y., Teng, C., Xia, R., and Meyers, B. C. (2020). PhasiRNAs in Plants: Their
694 Biogenesis, Genic Sources, and Roles in Stress Responses, Development, and
695 Reproduction. Plant Cell *32*, 3059-3080.
696 Llave, C., Kasschau, K. D., and Carrington, J. C. (2000). Virus-encoded suppressor of
697 posttranscriptional gene silencing targets a maintenance step in the silencing pathway.
698 Proc Natl Acad Sci U S A *97*, 13401-13406.
699 McGlincy, N. J., and Ingolia, N. T. (2017). Transcriptome-wide measurement of
700 translation by ribosome profiling. Methods *126*, 112-129.
701 Mine, A., Takeda, A., Taniguchi, T., Taniguchi, H., Kaido, M., Mise, K., and Okuno, T.
702 (2010). Identification and characterization of the 480-kilodalton template-specific RNA-
703 dependent RNA polymerase complex of *Red clover necrotic mosaic virus*. J Virol *84*,
704 6070-6081.
705 Montgomery, T. A., Howell, M. D., Cuperus, J. T., Li, D., Hansen, J. E., Alexander, A.
706 L., Chapman, E. J., Fahlgren, N., Allen, E., and Carrington, J. C. (2008). Specificity of
707 ARGONAUTE7-miR390 interaction and dual functionality in TAS3 trans-acting
708 siRNA formation. Cell *133*, 128-141.
709 Mourrain, P., Béclin, C., Elmayan, T., Feuerbach, F., Godon, C., Morel, J. B., Jouette,
710 D., Lacombe, A. M., Nikic, S., Picault, N., Rémoué, K., Sanial, M., Vo, T. A., and
711 Vaucheret, H. (2000). Arabidopsis SGS2 and SGS3 genes are required for
712 posttranscriptional gene silencing and natural virus resistance. Cell *101*, 533-542.
713 Muto, H., Nakatogawa, H., and Ito, K. (2006). Genetically encoded but nonpolypeptide
714 prolyl-tRNA functions in the A site for SecM-mediated ribosomal stall. Mol Cell *22*,
715 545-552.
716 Nakatogawa, H., and Ito, K. (2001). Secretion monitor, SecM, undergoes self-
717 translation arrest in the cytosol. Mol Cell *7*, 185-192.
718 Pall, G. S., and Hamilton, A. J. (2008). Improved northern blot method for enhanced
719 detection of small RNA. Nat Protoc *3*, 1077-1084.
720 Peragine, A., Yoshikawa, M., Wu, G., Albrecht, H. L., and Poethig, R. S. (2004). SGS3
721 and SGS2/SDE1/RDR6 are required for juvenile development and the production of
722 trans-acting siRNAs in Arabidopsis. Genes Dev *18*, 2368-2379.
723 Quinlan, A. R., and Hall, I. M. (2010). BEDTools: a flexible suite of utilities for
724 comparing genomic features. Bioinformatics *26*, 841-842.

Ruijtenberg, S., Sonneveld, S., Cui, T. J., Logister, I., de Steenwinkel, D., Xiao, Y., MacRae, I. J., Joo, C., and Tanenbaum, M. E. (2020). mRNA structural dynamics shape Argonaute-target interactions. Nat Struct Mol Biol *27*, 790-801.

Schuller, A. P., and Green, R. (2018). Roadblocks and resolutions in eukaryotic translation. Nat Rev Mol Cell Biol *19*, 526-541.

Stein, K. C., Kriel, A., and Frydman, J. (2019). Nascent Polypeptide Domain Topology and Elongation Rate Direct the Cotranslational Hierarchy of Hsp70 and TRiC/CCT. Mol Cell *75*, 1117-1130.e5.

Tomari, Y., and Iwakawa, H. O. (2017). In Vitro Analysis of ARGONAUTE-Mediated Target Cleavage and Translational Repression in Plants. Methods Mol Biol *1640*, 55-71.

Tsuzuki, M., Takeda, A., and Watanabe, Y. (2014). Recovery of dicer-like 1-late flowering phenotype by miR172 expressed by the noncanonical DCL4-dependent biogenesis pathway. RNA *20*, 1320-1327.

Vazquez, F., Vaucheret, H., Rajagopalan, R., Lepers, C., Gasciolli, V., Mallory, A. C., Hilbert, J. L., Bartel, D. P., and Crete, P. (2004). Endogenous trans-acting siRNAs regulate the accumulation of Arabidopsis mRNAs. Mol Cell *16*, 69-79.

Wu, H., Li, B., Iwakawa, H. O., Pan, Y., Tang, X., Ling-Hu, Q., Liu, Y., Sheng, S., Feng, L., Zhang, H., Zhang, X., Tang, Z., Xia, X., Zhai, J., and Guo, H. (2020). Plant 22-nt siRNAs mediate translational repression and stress adaptation. Nature *581*, 89-93.

Yanagitani, K., Kimata, Y., Kadokura, H., and Kohno, K. (2011). Translational pausing ensures membrane targeting and cytoplasmic splicing of XBP1u mRNA. Science *331*, 586-589.

Yoshikawa, M., Iki, T., Numa, H., Miyashita, K., Meshi, T., and Ishikawa, M. (2016). A Short Open Reading Frame Encompassing the MicroRNA173 Target Site Plays a Role in trans-Acting Small Interfering RNA Biogenesis. Plant Physiol *171*, 359-368.

Yoshikawa, M., Iki, T., Tsutsui, Y., Miyashita, K., Poethig, R. S., Habu, Y., and Ishikawa, M. (2013). 3' fragment of miR173-programmed RISC-cleaved RNA is protected from degradation in a complex with RISC and SGS3. Proc Natl Acad Sci U S A *110*, 4117-4122.

Zhang, C., Ng, D. W., Lu, J., and Chen, Z. J. (2012). Roles of target site location and sequence complementarity in trans-acting siRNA formation in Arabidopsis. Plant J *69*, 217-226.

758 Zhang, K., Zhang, X., Cai, Z., Zhou, J., Cao, R., Zhao, Y., Chen, Z., Wang, D., Ruan,
759 W., Zhao, Q., Liu, G., Xue, Y., Qin, Y., Zhou, B., Wu, L., Nilsen, T., Zhou, Y., and Fu,
760 X. D. (2018). A novel class of microRNA-recognition elements that function only
761 within open reading frames. Nat Struct Mol Biol *25*, 1019-1027.

762

Acknowledgements

We thank James Carrington for providing *Nicotiana benthamiana* seed, *Agrobacterium tumefaciens* GV3101, pMDC32, pMDC32-3×HA-AGO7, pMDC32-TAS3a and a detailed protocol for *Agrobacterium* infiltration, Yukio Kurihara for *Arabidopsis thaliana* (Col-0) seeds, Koreaki Ito and Yuhei Chadani for helpful advice on neutral pH gel electrophoresis analyses, Yuichi Shichino and Mari Mito for technical assistance on ribosome profiling, Keisuke Shoji for kind advice and assistance on NGS data analyses, and Kyungmin Baeg and Yayoi Endo for plasmid construction. We also thank all the members of the Tomari laboratory for discussion and critical comments on the manuscript. We also thank Life Science Editors for editorial assistance. This work was supported in part by JST, PRESTO (grant JPMJPR18K2 to H.-o.I.), Grant-in-Aid for Scientific Research on Innovative Areas ('Nascent-chain Biology') (grant 26116003 to H.-o.I.), and Grant-in-Aid for Scientific Research (B) (grant 18H02380 to M.Y.). DNA libraries were sequenced by the Vincent J. Coates Genomics Sequencing Laboratory at UC Berkeley, supported by an NIH S10 OD018174 Instrumentation Grant.

Author Contributions

H.-o.I. conceived of the project and designed the experiments; H.-o.I. and T.F. performed ribosome profiling and bioinformatic analyses with the supervision of S.I; H.-o.I., A.L., and K.K. performed biochemical analyses; A.M. and A.T. performed transient expression assays in *Nicotiana benthamiana*; H.-o.I., S.I. and Y.T. wrote the manuscript with editing from all the authors; all the authors discussed the results and approved the manuscript.

Competing interests

Authors declare no competing interests.

Corresponding author

Correspondence and requests for materials should be addressed to Hiro-oki Iwakawa (iwakawa@iqb.u-tokyo.ac.jp)

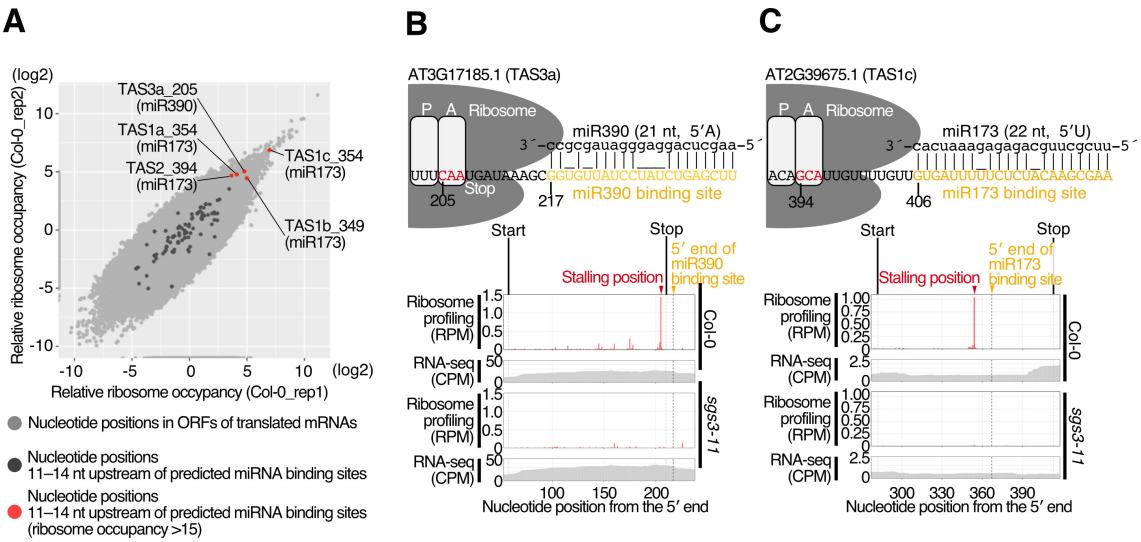

Figure 1. The dsRNA-binding protein SGS3 promotes microRNA-mediated ribosome stalling. (A) Scatter plot showing correlation of relative ribosome occupancy (Materials and Methods) between replicates (Col-0_rep1 and 2). The nucleotide positions with ribosome footprints (reads per million (RPM) over 0.05) in translating ORFs are shown in light gray. The nucleotide positions 11–14 nucleotide upstream of predicted miRNA binding sites are shown in dark gray (Table S1). In such positions, those with relative ribosome occupancy over 15 are shown in red (Table S1). (B, C) Ribosome footprints (A-site position) in RPM and RNA-seq in coverage per million (CPM) in wild-type or *sgs3-11* mutant seedlings are shown for the following transcripts: (B) AT3G17185.1 (TAS3a), a precursor of trans acting siRNAs (tasiRNAs) with miR390 binding sites; (C) AT2G39675.1 (TAS1c), a precursor of tasiRNAs with a miR173 binding site. See also Figure S1 and Table S1.

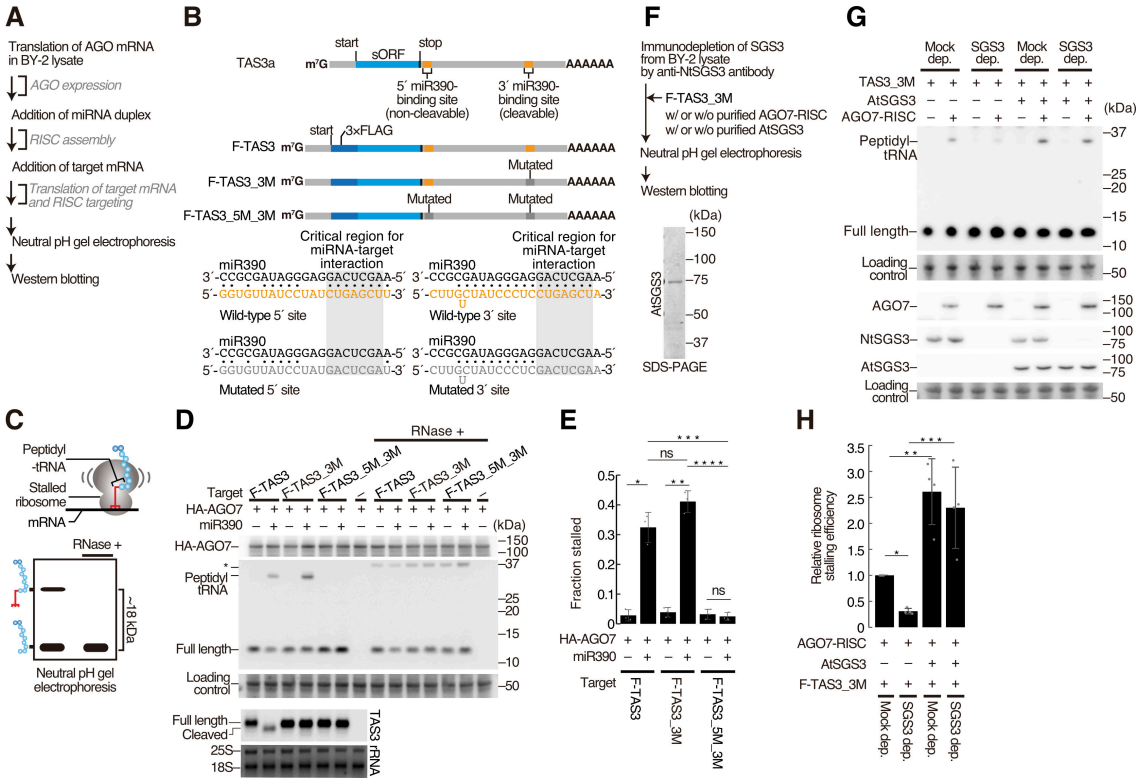

Figure 2. *In vitro* recapitulation of microRNA-mediated ribosome stalling.
(A) Flowchart of the miRNA-mediated ribosome stalling assay *in vitro*. (B) (top) Schematic representation of TAS3a RNA and its 3×FLAG-tag fused variants. The orange and gray boxes indicate wild-type and mutated miR390-binding sites, respectively. (bottom) The base-pairing configurations between miR390 and the wild-type or mutated miR390-binding sites. The critical regions for the miRNA-target interaction are shown in the shaded boxes. (C) Schematic representation of SDS-PAGE in a neutral pH environment, to thus detect peptidyl-tRNAs. (D) Both AGO7-RISC and the 5′ binding site are required for ribosome stalling *in vitro*. After *in vitro* silencing assay, half of the reaction mixture was treated with RNase (RNase +), and used for PAGE followed by Western blotting. The full-length polypeptide and peptidyl-tRNA were detected by anti-FLAG antibody. 3×HA-AGO7 (HA-AGO7) was detected by anti-HA antibody. Total protein was stained using Ponceau S, and the ~50 kDa bands were used as a loading control. The asterisk indicates the positions of the unexpected protein bands that appears with RNase treatment. (bottom) Northern blotting of TAS3 variants. Methylene blue-stained rRNA was used as a loading control. (E) Quantification of ribosome stalling efficiencies in (D). Fraction stalled was calculated using the following formula: Fraction stalled = peptidyl-tRNA/(full-length + peptidyl-tRNA). The mean values ± SD from three independent experiments are shown. Bonferroni-corrected P values from two-sided paired t-tests are as follows: *P = 0.03361; **P = 0.03817; ***P = 0.03809, ****P = 0.03174. (F) (top) Flowchart of the *in vitro* miRNA-mediated ribosome stalling assay with SGS3-immunodepleted lysate. (bottom) Coomassie brilliant blue staining of purified AtSGS3. (G) SGS3 promotes miRNA-mediated ribosome stalling *in vitro*. Endogenous NtSGS3, recombinant AtSGS3, and recombinant AGO7 were detected using anti-NtSGS3, anti-AtSGS3, and anti-AtAGO7 antibodies, respectively. See also Figure 2D legend. (H) Quantification of relative ribosome stalling efficiencies in (G). The signal intensity of peptidyl-tRNA/(full-length + peptidyl-tRNA) was normalized to the value of Mock dep. (AtSGS3 –). The mean values ± SD from four independent experiments are shown. Bonferroni-corrected P values from two-sided paired t-tests are as follows: *P = 0.00039; **P = 0.04433; ***P = 0.03889.

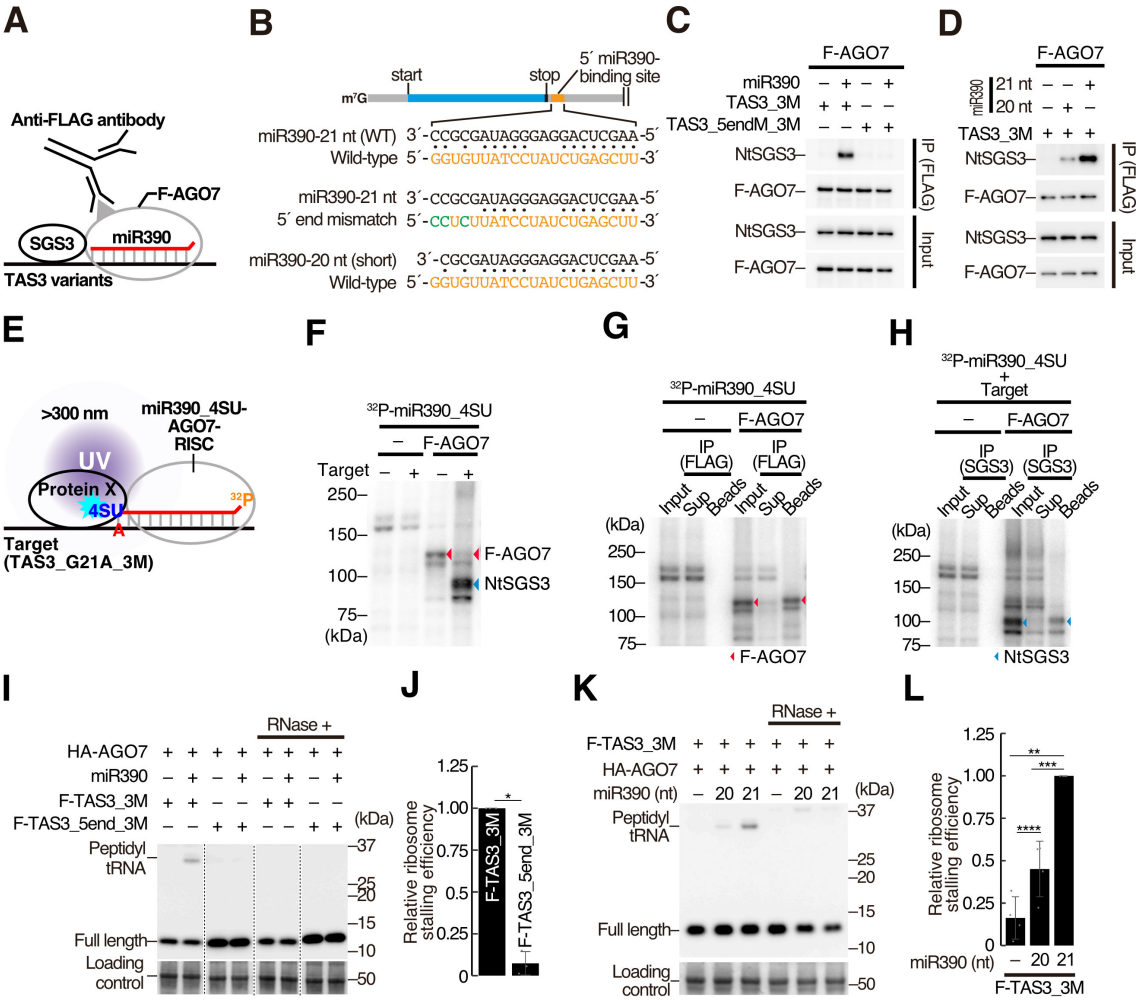

Figure 3. SGS3 binding to the 3′ end of miR390 is required for the ribosome pausing.

(A) Schematic representation of co-immunoprecipitation assay with anti-FLAG antibody in the presence of F-AGO7, miR390, and TAS3 variants. (B) Base-pairing configurations. (top) miR390 and wild-type 5′ miR390-binding site. (middle) miR390 and 5′ site with 5′ end mismatches (5endM). (bottom) 20-nt miR390 and the wild-type 5′ site. The mutated nucleotides are shown in green. (C) 5′ end mismatches in the 5′ site disrupt interaction between SGS3 and AGO7. (D) The use of a short miR390 variant (20 nt) disrupted interaction between SGS3 and AGO7. (E) An overview of the UV crosslink experiment. AGO7 was programmed with the 5′-radiolabeled miR390 variant bearing the 3′ 4-thio-U (^{32}P-miR390_4SU) in BY-2 lysate, and further incubated with the TAS3 variant (TAS3_G21A_3M). The reaction mixture was analyzed using 10% SDS-PAGE and crosslinked proteins were detected using phosphorimaging. The ellipse indicates neighboring proteins. (F) miR390-loaded AGO7 directly interacts with NtSGS3 in the presence of TAS3_G21A_3M. 5′ end-radiolabeled miR390 with a 3′ 4-thio-U was incubated in BY-2 lysate in the presence or absence of F-AGO7 and target RNA (TAS3_G21A_3M), crosslinked by UV light (>300 nm), then analyzed by SDS-PAGE. The red and blue arrowheads indicate AGO7 and NtSGS3, respectively (See also g and h). (G) Detection of F-AGO7 by UV crosslinking. The 5′ end-radiolabeled miR390 with a 3′ 4-thio-U was incubated in BY-2 lysate in the presence of F-AGO7, crosslinked by UV light (>300 nm), immunoprecipitated using anti-FLAG antibody, and then analyzed by SDS-PAGE. F-AGO7 was efficiently crosslinked to 4-thio-U at the 3′ end of miR390. (H) Detection of NtSGS3 by UV crosslinking. 5′ end-radiolabeled miR390 with a 3′ 4-thio-U was incubated in BY-2 lysate in the presence of F-AGO7 and target RNA (TAS3_G21A_3M), crosslinked by UV light (>300 nm), immunoprecipitated by anti-NtSGS3 antibody, and then analyzed by SDS-PAGE. NtSGS3 was

854 efficiently crosslinked to 4-thio-U at the 3′ end of miR390 in the presence of the target RNA. (I) and
855 (K) *in vitro* ribosome stalling experiments. Mismatches at the 5′ end of miR390-binding site or the use
856 of 20-nt miR390 decreased stalled ribosomes. See also the legend of Figure 2D. (J) and (L)
857 Quantification of relative ribosome stalling efficiencies in (I) and (K), respectively. The signal
858 intensity of peptidyl-tRNA/(full-length + peptidyl-tRNA) was normalized to the value of F-TAS3_3M
859 (I) or miR390 (21 nt) (K). The mean values ± SD from three (J) and four (L) independent experiments
860 are shown, respectively. P value from two-sided paired t-tests are as follows: *P = 0.00190 (J).
861 Bonferroni-corrected P values from two-sided paired t-tests are as follows: **P = 0.00270; ***P =
862 0.02034; ****P = 0.04343 (L).
863

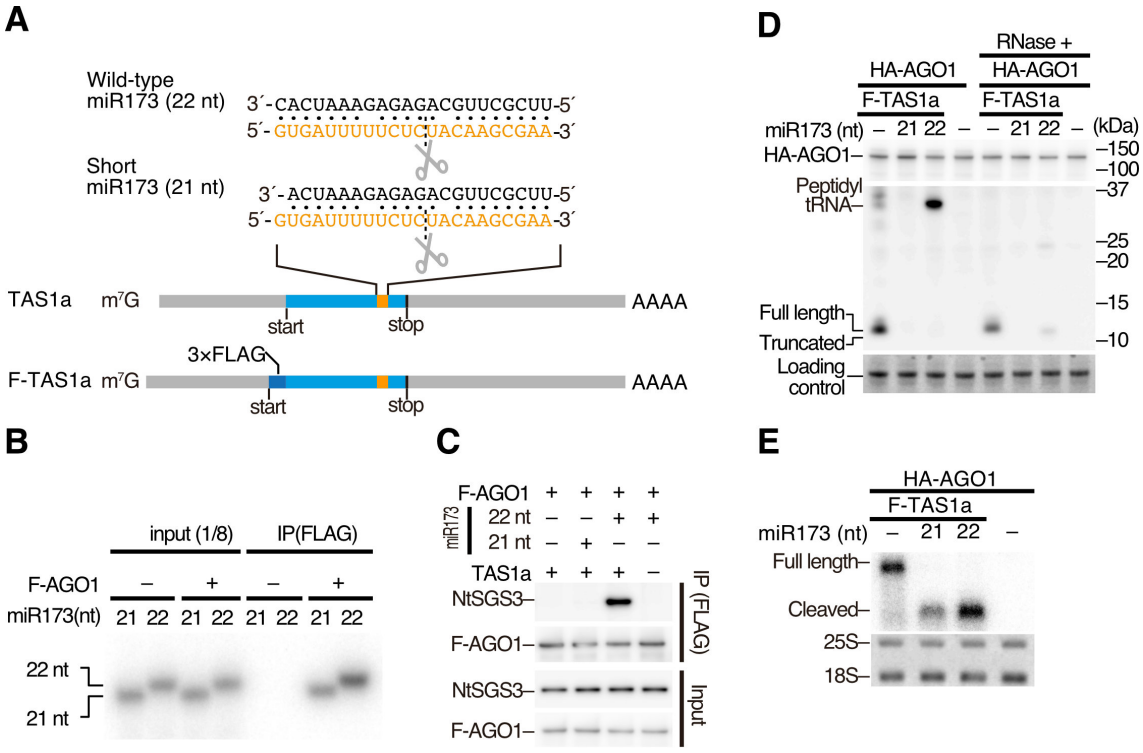

Figure 4. AGO1 loaded with 22-nt miR173 efficiently stalls ribosome. (A) (top) Base-pairing configurations between 22/21-nt miR173 and the miR173-binding site in TAS1a. (bottom) Schematic representation of TAS1a RNA and its 3×FLAG-tag fused variant. (B) *In vitro* RISC assembly with AGO1 and radiolabeled 21 and 22-nt miR173 duplexes. After translation of 3×FLAG-AGO1 (F-AGO1) mRNA *in vitro*, the radiolabeled miR173 duplex was added and further incubated for RISC assembly. Then, F-AGO1 was immunoprecipitated with anti-FLAG antibody. The co-immunoprecipitated miR173 was analyzed by denaturing PAGE. Both 21- and 22-nt miR173 duplexes were incorporated into AGO1. (C) Co-immunoprecipitation experiments with 3×FLAG-AGO1 in the presence of 21 or 22-nt miR173 duplex and TAS1a RNA. AGO1-RISC loaded with 22-nt miR173 interacts with NtSGS3 in the presence of TAS1a RNA. In contrast, 21-nt miR173 failed to promote the interaction between AGO1 and NtSGS3. (D) *In vitro* ribosome stalling experiments. Peptidyl-tRNA was accumulated in the presence of AGO1-RISC loaded with 22-nt miR173, while no peptidyl-tRNA was observed in the presence of that with 21-nt miR173. (E) Northern blotting of TAS1 reporter RNAs. TAS1 was efficiently cleaved by AGO1-RISC loaded with 21- and 22-nt miR173. Methylene blue-stained rRNA was used as a loading control.

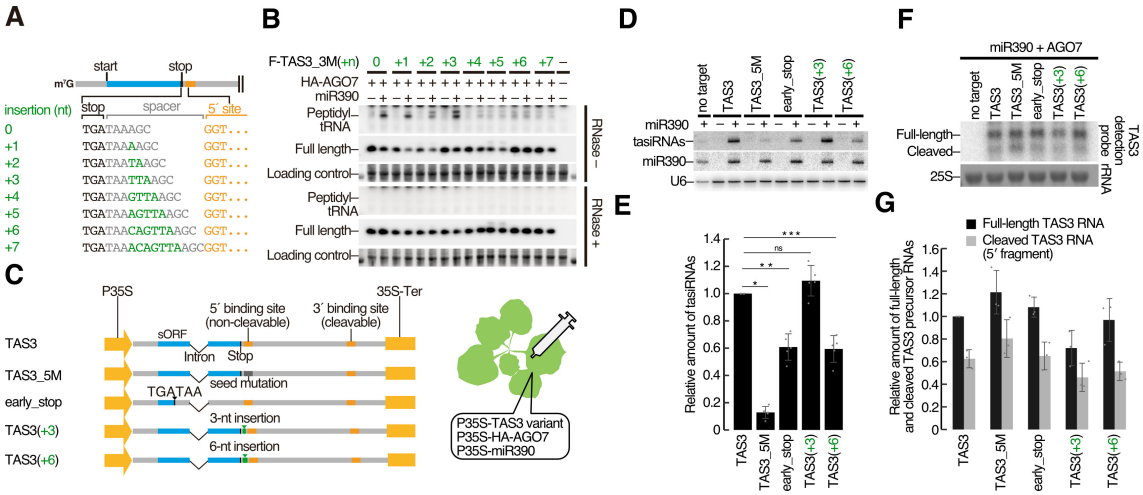

Figure 5. Ribosome stalling is not an essential event but an enhancer for the production of secondary siRNAs.

(A) Schematic representation of TAS3 variants with different nucleotide insertions (green) between the stop codon (black) and the 5′ miR390-binding site (orange). (B) *In vitro* ribosome stalling experiments. Insertions of over 3 nucleotides decreased stalled ribosomes. After *in vitro* silencing assay, half of the reaction mixture was treated with RNase (RNase +), and used for PAGE followed by Western blotting. The full-length polypeptide and peptidyl-tRNA were detected by anti-FLAG antibody. Total protein was stained using Ponceau S, and the ~50 kDa bands were used as a loading control. (C) Schematic representation of plasmids carrying TAS3 variants used in the *Nicotiana benthamiana (N. benthamiana)* transient assay. P35S and 35S-Ter indicate Cauliflower mosaic virus (CaMV) 35S promoter and terminator, respectively. Leaves of *N. benthamiana* plants were infiltrated with a mixture of *Agrobacterium tumefaciens* cultures harboring P35S-HA-AGO7, P35S-TAS3 variants, and P35S-miR390 or empty vector. Leaves were harvested at 2-day post infiltration and used for Northern blotting to detect secondary siRNAs and the sense strand of TAS3 mRNAs. (D) Northern blotting of secondary siRNAs from TAS3 and its variants, miR390, and U6 RNAs. (E) Quantification of the secondary siRNAs in (D). The signal intensity of tasiRNAs was calibrated with miR390, and normalized to the value of TAS3 (miR390 +). The mean values ± SD from five independent experiments are shown. Bonferroni-corrected P values from two-sided paired t-tests are as follows: *P = 5.96313E-06; **P = 0.00332; ***P = 0.00329. A positive correlation was observed between tasiRNA biogenesis and miR390-mediated ribosome stalling. (F) Northern blotting of the full-length TAS3 RNAs and the 5′ cleaved fragments. Methylene blue-stained rRNA was used as a loading control. (G) The signal intensity of TAS3 RNA/rRNA was normalized to the value of full-length TAS3. The mean values ± SD from three independent experiments are shown. No correlation was observed between ribosome stalling and accumulation of the sense strand of TAS3 RNAs.

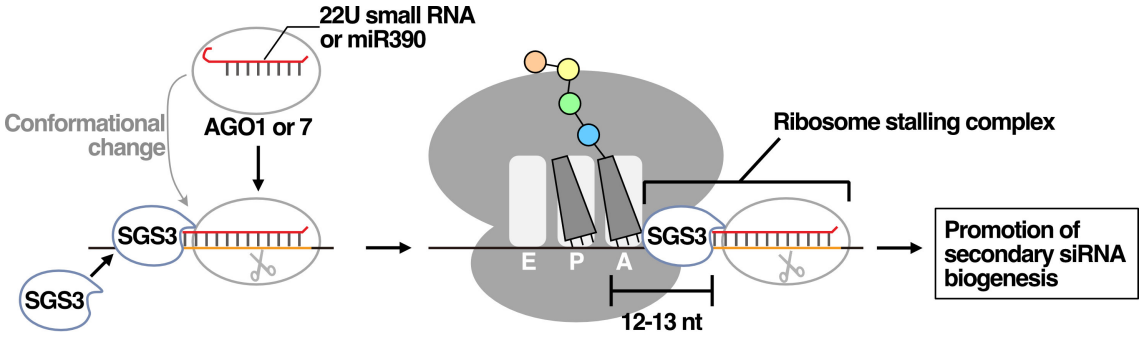

Figure 6. A model for ribosome stalling caused by SGS3-miRNA-Argonaute complex and its role in secondary siRNA biogenesis.

Target binding causes dynamic conformational changes in 22U-AGO1-RISC or miR390-AGO7-RISC, resulting in protrusion of the 3′ end of the small RNA from the RISC complex. SGS3 directly binds the dsRNA formed between the 3′ side of the small RNA and the 5′ side of the target site. The SGS3-small RNA complex stalls ribosomes at 12–13 nt upstream of the binding sites. This ribosome stalling stimulates secondary siRNA production in a manner different from mRNA stabilization.

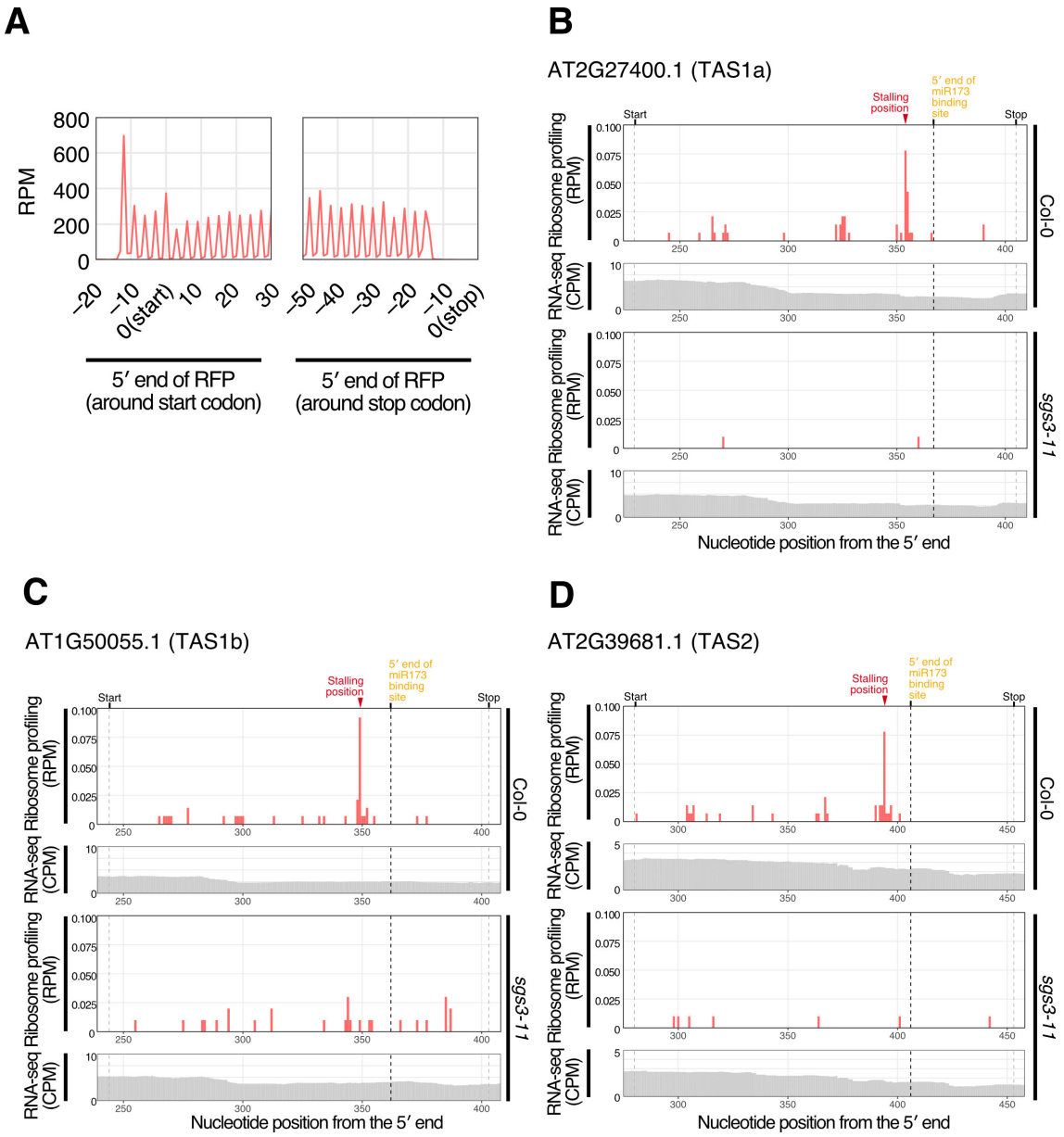

Figure S1. Representative ribosome stalling positions with a downstream miRNA-binding site. (A) Ribosome occupancies around start (left) and stop (right) codons using 28 nt foot prints for 3 day old seedlings of wild-type *Arabidopsis thaliana* (Col-0). The traces indicate 5′ end of ribosome footprints. Ribosome footprints (A-site positions) in RPM and RNA-seq in CPM in 3 day old wild-type or *sgs3-11* mutant seedlings are shown for the following transcripts: (B) AT2G27400.1 (TAS1a), encoding one of the isoforms of TAS1; (C) AT1G50055.1 (TAS1b) encoding one of the isoforms of TAS1; (D) AT2G39681.1 (TAS2) encoding a precursor of tasiRNAs with a miR173 binding site. Related to Figure 1B and C.

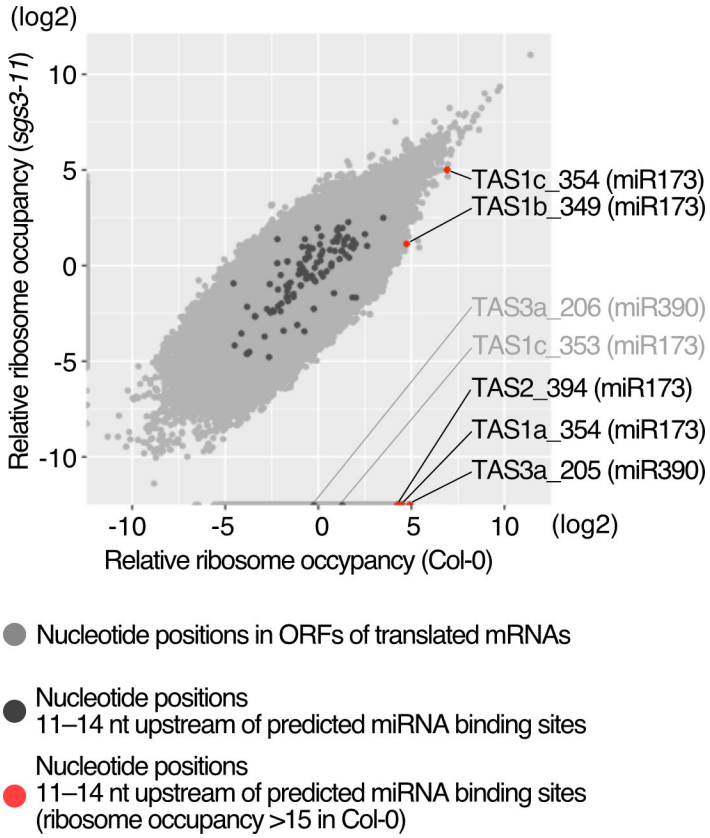

926
927 **Figure S2. SGS3 is not a general ribosome stalling factor, but rather a specific stalling**
928 **enhancer for miRNA-mediated ribosome stalling.**
929 A scatter plot shows the relative ribosome occupancy (Materials and Methods) between Col-0 and
930 *sgs3-11* seedlings. The nucleotide positions with ribosome footprints (RPM over 0.05 in Col-0 or *sgs3-*
931 *11*) in translating ORFs are shown in light gray. See also the legend of Figure 1A.
932

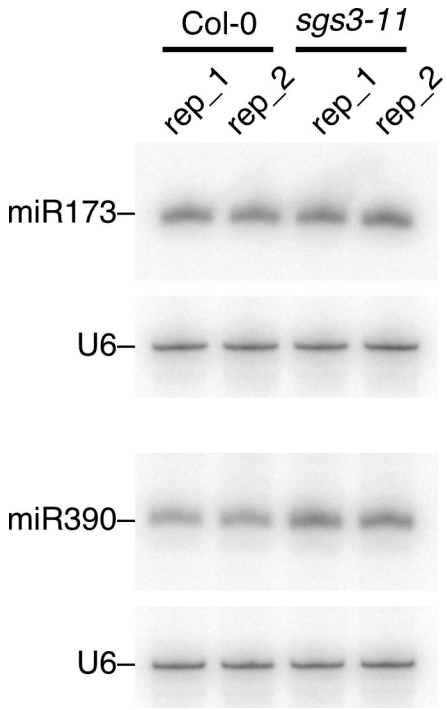

Figure S3. miR173 and miR390 abundance in Col-0 and *sgs3-11* seedlings.
miR173 and miR390 in wild-type (Col-0) and *sgs3-11* seedlings were detected by Northern blotting. U6 RNA was used as a loading control.

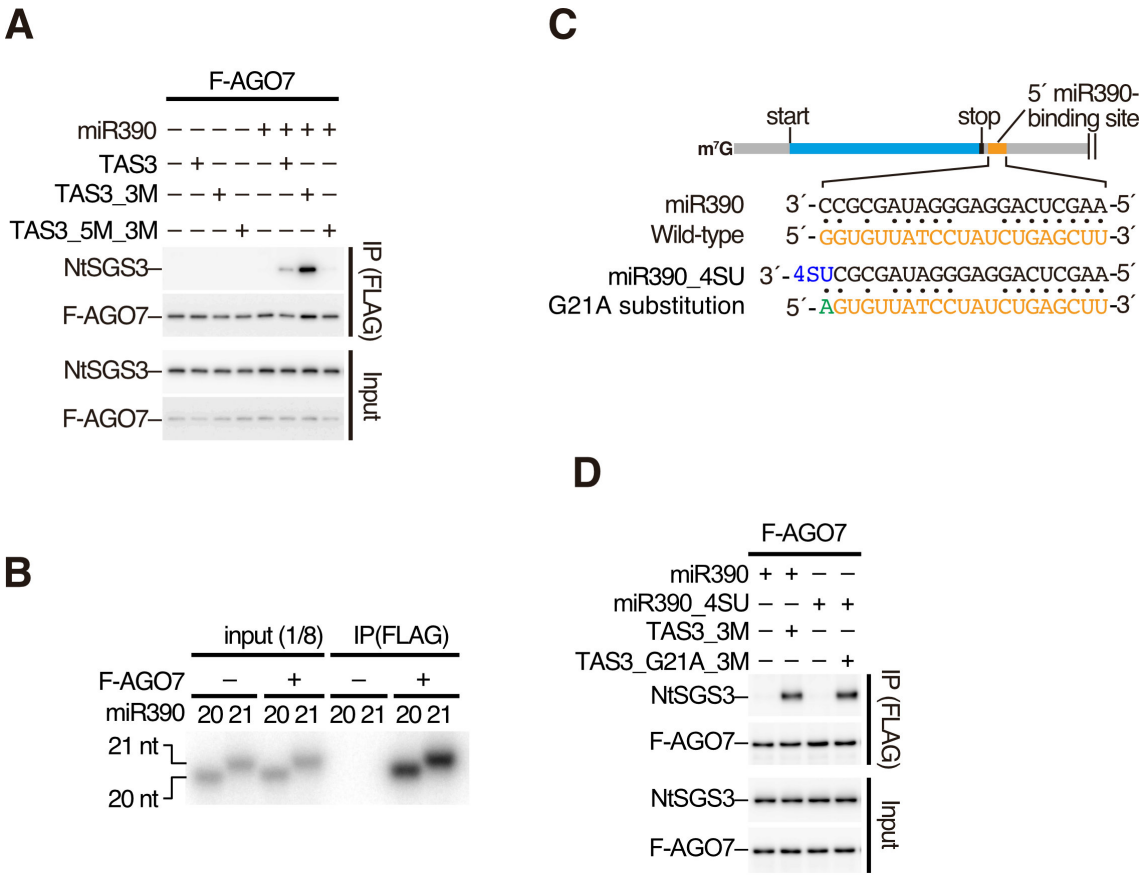

Figure S4. Co-immunoprecipitation of NtSGS3 with AGO7 in the presence of TAS3 variants, and AGO7-RISC assembly with 21-nt and 20-nt miR390. (A) NtSGS3 was specifically co-immunoprecipitated with F-AGO7 in the presence of miR390 duplex and TAS3 or the TAS3-3M. The reason why more SGS3 was co-immunoprecipitated in TAS3_3M than wild-type TAS3 is because the wild-type TAS3 mRNA is cleaved at the 3′ binding site by AGO7-RISC, thereby destabilized in the lysate as shown in Figure 2D. (B) *In vitro* RISC assembly with F-AGO7 and radiolabeled 20 and 21-nt miR390 duplexes. After RISC assembly, F-AGO7 was immunoprecipitated with anti-FLAG antibody. The co-immunoprecipitated miR390 was analyzed by denaturing PAGE. Both 20- and 21-nt miR390 duplexes were efficiently incorporated into AGO7. (C) Schematic of base-pairing configurations between miR390-4SU and a 5′ miR390-binding site with a G21A substitution. The mutated nucleotides in TAS3 variant are shown in green. 4-thiouridine is shown in blue. (D) AGO7-RISC loaded with 21-nt miR390 variant possessing 4-thiouridine at the 3′ end (miR390_4SU) efficiently interacts with NtSGS3 in the presence of TAS3 variant with a compensatory G-to-A mutation at the 5′ end of miR390 binding site (TAS3_G21A_3M).

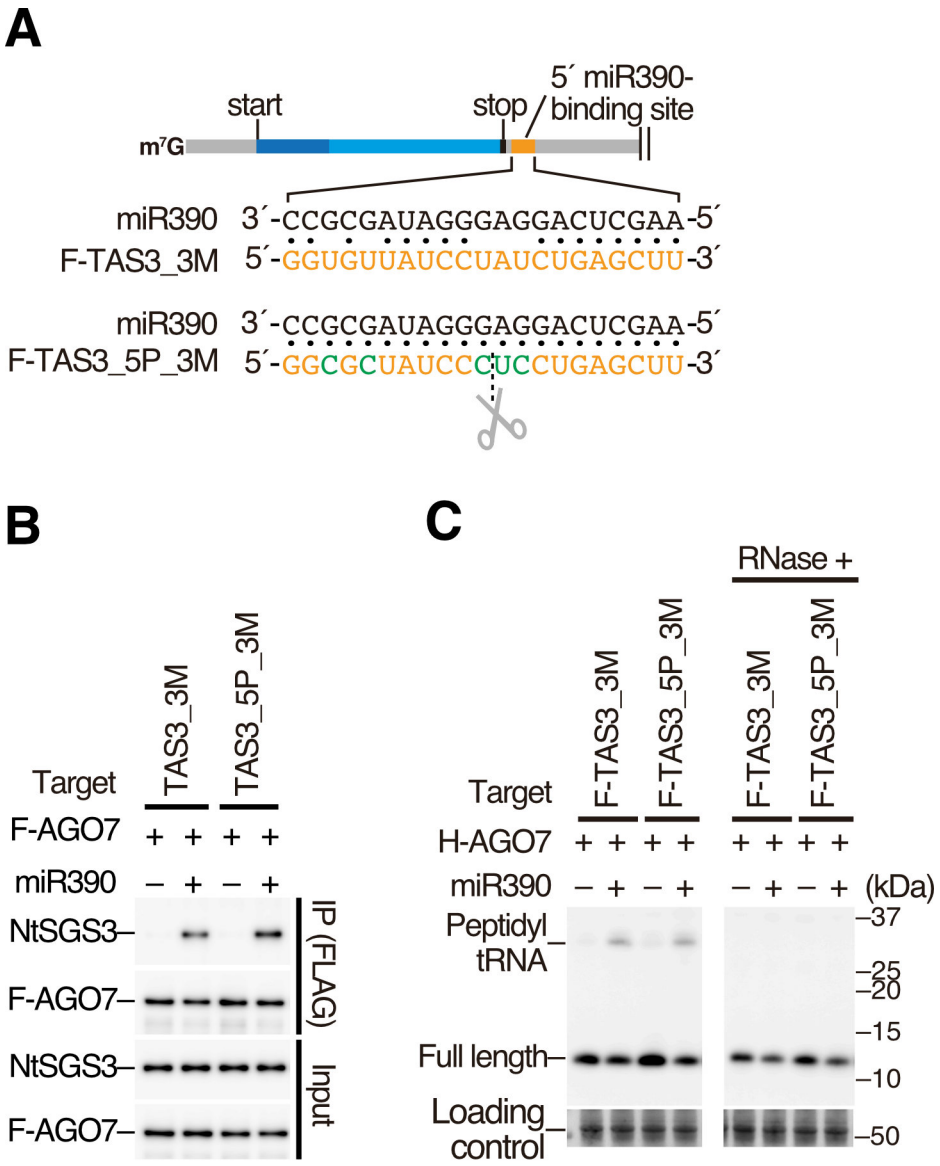

Figure S5. A cleavable target site facilitates ribosome stalling mediated by the miR390-AGO7 RISC. (A) Schematic of base-pairing configurations between miR390 and a 5′ target site with perfect complementarity to miR390. The mutated nucleotides in the TAS3 variant (F-TAS3_5P_3M) are shown in green. (B) Co-immunoprecipitation experiments. AGO7-RISC efficiently interacts with SGS3 in the presence of a F-TAS3_3M variant with a 5′ target site with perfect complementarity to miR390 (F-TAS3_5P_3M). (C) *In vitro* ribosome stalling experiments. Peptidyl-tRNA was accumulated in the presence of AGO7-RISC and F-TAS3_5P_3M, suggesting that cleavable site facilitates ribosome stalling mediated by miR390-AGO7-RISC.

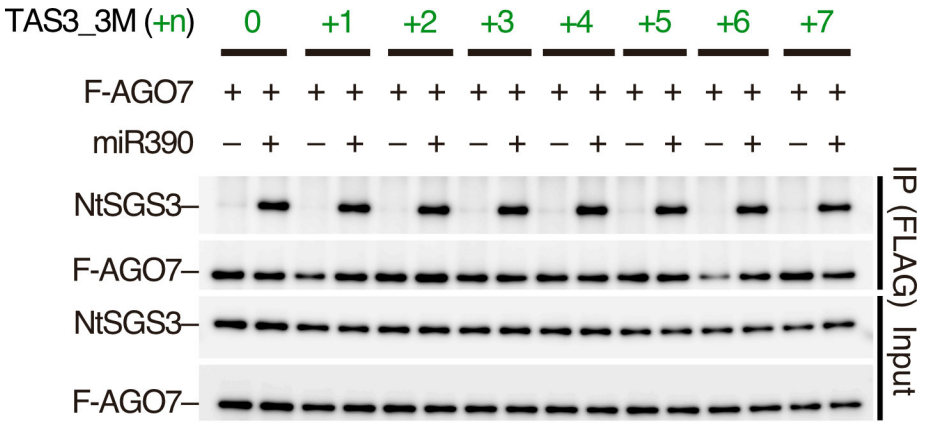

Figure S6. Nucleotide insertion between the stop codon and the 5′ miR390 binding site has no effect on the interaction between AGO7 and NtSGS3. NtSGS3 was specifically and efficiently co-immunoprecipitated with F-AGO7 in the presence of miR390 duplex and TAS3 variants with nucleotide insertions between the stop codon and the 5′ miR390-binding site.

974 **Table S1. Nucleotide positions 11–14 nt upstream of predicted miRNA binding sites.**
975
976 **Table S2. List of TAS3 homologs.**
977
978 **Table S3. List of synthetic RNA oligos used in this study.**
979
980 **Table S4. List of synthetic DNA oligos and long DNA fragments used in this study.**
981

Supplementary Table 1. Nucleotide positions 11–14 nt upstream of predicted miRNA binding sites.

ID	Acc.	A_site	Occupancy_Col-0_rep	Occupancy_Col-0_r	Occupancy_Col-0	Occupancy_*sgs3-11*_rep	Occupancy_*sgs3-11*_rep	Occupancy_*sgs3*	miRNA_Acc.	Expectation	miRNA_start	miRNA_end	Target_start	Target_end	miRNA_aligned_fragment	Target_aligned_fragment	Target_Desc.	distance_A_site_target_site	occupancy_ratio (*sgs3-11*/Col-0)
AT2G39675.1_354	AT2G39675.1	354	124.9047619	116.90625	120.905506	21.5	43	32.25	ath-miR173-5p	1.5	1	22	367	388	UUCGCUUGCAGAGAGAAAUCAC	GUGAUUUUUCUCUACAAGCGAA	| Symbols: TAS1C | TAS1C; other RN	13	0.266737232
AT3G17185.1_205	AT3G17185.1	205	27.38095238	32.93413174	30.15754206	0	0	0	ath-miR390a	3	1	21	217	237	AAGCUCAGGAGGGAUAGCGCC	GGUGUUAUCCUAUCUGAGCUU	| Symbols: TASIR-ARF, TAS3, ATT	12	0
AT1G50055.1_349	AT1G50055.1	349	31.8	21.82352941	26.81176471	0	4.416666667	2.208333333	ath-miR173-5p	2.5	1	22	362	383	UUCGCUUGCAGAGAGAAAUCAC	GUGAUUUUUCUCAACAAGCGAA	| Symbols: TAS1B | TAS1B; other RN	13	0.082364341
AT2G27400.1_354	AT2G27400.1	354	17.4	27.29411765	22.34705882	0	0	0	ath-miR173-5p	1.5	1	22	367	388	UUCGCUUGCAGAGAGAAAUCAC	GUGAUUUUUCUCUACAAGCGAA	| Symbols: TAS1A | TAS1A; other RI	13	0
AT2G39681.1_394	AT2G39681.1	394	12.66666667	25.65	19.15833333	0	0	0	ath-miR173-5p	1.5	1	22	406	427	UUCGCUUGCAGAGAGAAAUCAC	GUGAUUUUUCUCUCCAAGCGAA	| Symbols: TAS2 | TAS2; other RNA	12	0
AT4G37150.1_725	AT4G37150.1	725	10.92266667	11.55234657	11.23750662	4.48	6.826666667	5.653333333	ath-miR5595a	1	1	21	738	758	ACAUAUGAUCUGCAUCUUUGC	UCAAAGAUGCAGAUCAUAUGC	| Symbols: ATMES9, MES9 | methyl	13	0.503077197
AT3G10160.1_778	AT3G10160.1	778	6.12745098	6.188118812	6.157784896	4.08496732	0	2.04248366	ath-miR865-3p	2.5	1	21	790	810	UUUUUCCUCAAAUUUAUCCAA	UUGGAUAUAUCUGAGGAAAAG	| Symbols: ATDFC, DFC, FPGS2 | D	12	0.331691297
AT1G52070.1_340	AT1G52070.1	340	5.461956522	5.878940731	5.670448627	2.70723593	3.540372671	3.1238043	ath-miR846	2.5	1	21	354	374	UUGAAUUGAAGUGCUUGAAUU	GAUGCAAGCACUUGAAUUCAA	| Symbols: | Mannose-binding lectin s	14	0.550891915
AT2G36400.1_732	AT2G36400.1	732	5.420233463	2.685560054	4.052896759	0.627760252	0	0.313880126	ath-miR396a	3	1	21	746	767	UUCCACA-GCUUUCUUGAACUG	CCGUUCAAGAAAGCCUGUGGAA	| Symbols: AtGRF3, GRF3 | growth-r	14	0.077445873
AT1G19540.1_598	AT1G19540.1	598	3.415977961	4.626865672	4.021421817	3.315508021	1.09540636	2.205457191	ath-miR868-3p	3	1	21	609	629	CUUCUUAAGUGCUGAUAAUGC	CCAUUGUCAACACUGAAGAAG	| Symbols: | NmrA-like negative trans	11	0.548427221
AT1G60430.1_361	AT1G60430.1	361	2.676923077	4.68161435	3.679268713	3.824175824	0	1.912087912	ath-miR5020b	2	1	21	375	395	AUGGCAUGAAAGAAGGUGAGA	AAUCACCUUCUUUCGUGCUAA	| Symbols: ARPC3 | actin-related prot	14	0.519692379
AT1G60430.1_361	AT1G60430.1	361	2.676923077	4.68161435	3.679268713	3.824175824	0	1.912087912	ath-miR5020c	2.5	1	21	374	394	UGGCAUGGAAGAAGGUGAGAC	CAAUCACCUUCUUUCGUGCUA	| Symbols: ARPC3 | actin-related prot	13	0.519692379
AT1G60430.2_394	AT1G60430.2	394	2.676923077	4.68161435	3.679268713	3.824175824	0	1.912087912	ath-miR5020b	2	1	21	408	428	AUGGCAUGAAAGAAGGUGAGA	AAUCACCUUCUUUCGUGCUAA	| Symbols: ARPC3 | actin-related prot	14	0.519692379
AT1G60430.2_394	AT1G60430.2	394	2.676923077	4.68161435	3.679268713	3.824175824	0	1.912087912	ath-miR5020c	2.5	1	21	407	427	UGGCAUGGAAGAAGGUGAGAC	CAAUCACCUUCUUUCGUGCUA	| Symbols: ARPC3 | actin-related prot	13	0.519692379
AT4G29950.2_980	AT4G29950.2	980	4.439150402	2.883511075	3.661330738	3.175607002	1.331439394	2.253523198	ath-miR5634	3	1	21	991	1011	AGGGACUUUGUGAAUUUAGGG	CUUUGAAUUCAAAAAGUUUCU	| Symbols: | Ypt/Rab-GAP domain of	11	0.615492934
AT5G03455.1_268	AT5G03455.1	268	4.626760563	2.678899083	3.652829823	3.804560261	1.201646091	2.503103176	ath-miR5646	3	1	20	281	300	GUUCGAGGCACGUUGGGAGG	UCUUCCAUUGUGCCUUGAGC	| Symbols: CDC25, ARATH;CDC25,	13	0.685250421
AT4G37150.1_724	AT4G37150.1	724	5.347258486	1.780869565	3.564064025	0.630541872	0	0.315270936	ath-miR5595a	1	1	21	738	758	ACAUAUGAUCUGCAUCUUUGC	UCAAAGAUGCAGAUCAUAUGC	| Symbols: ATMES9, MES9 | methyl	14	0.088458269
AT4G29950.1_987	AT4G29950.1	987	3.94627383	2.670106417	3.308190124	2.825938567	1.171145686	1.998542126	ath-miR5634	3	1	21	998	1018	AGGGACUUUGUGAAUUUAGGG	CUUUGAAUUCAAAAAGUUUCU	| Symbols: | Ypt/Rab-GAP domain of	11	0.604119489
AT5G04200.1_1079	AT5G04200.1	1079	4.452054795	1.829268293	3.140661544	0	2.671232877	1.335616438	ath-miR5029	3	1	21	1092	1112	AAUGAGAGAGAACACUGCAAA	UUUGCGUUGUUUUCUUUUAUU	| Symbols: AtMC9, MC9 | metacaspa	13	0.425265957
AT4G34090.3_493	AT4G34090.3	493	2.356495468	3.754512635	3.055504052	3.842364532	5.811258278	4.826811405	ath-miR5636	3	1	21	505	525	CGUAGUUGCAGAGCUUGACGG	UCGUCAGGCUCUGUUACUGCG	| Symbols: | unknown protein; FUNC	12	1.57971036
AT3G51270.2_333	AT3G51270.2	333	1.982683983	3.920114123	2.951399053	2.726190476	2.871473354	2.798831915	ath-miR5631	2.5	1	21	346	366	UGGCAGGAAAGACAUAAUUUU	UGGGUUAUGACUUUCUUGCCA	| Symbols: | protein serine/threonine k	13	0.948306842
AT3G51270.1_307	AT3G51270.1	307	1.941052632	3.794238683	2.867645657	2.609433962	2.777108434	2.693271198	ath-miR5631	2.5	1	21	320	340	UGGCAGGAAAGACAUAAUUUU	UGGGUUAUGACUUUCUUGCCA	| Symbols: | protein serine/threonine k	13	0.939192467
AT3G17185.1_204	AT3G17185.1	204	3.06122449	2.462121212	2.761672851	1.818181818	1.162790698	1.490486258	ath-miR390a	3	1	21	217	237	AAGCUCAGGAGGGAUAGCGCC	GGUGUUAUCCUAUCUGAGCUU	| Symbols: TASIR-ARF, TAS3, ATT	13	0.539704135
AT1G77330.1_628	AT1G77330.1	628	3.857354028	1.407795611	2.632574819	2.196644461	2.768179174	2.482411817	ath-miR3933	2.5	1	21	639	659	AGAAGCAAAAUGACGACUCGG	AGGAGGUGUCGUUUUGCUUUU	| Symbols: | 2-oxoglutarate (2OG) and	11	0.942959645
AT1G52060.1_340	AT1G52060.1	340	4.577259475	0.667375133	2.622317304	2.13787234	2.128813559	2.13334295	ath-miR846	2.5	1	21	354	374	UUGAAUUGAAGUGCUUGAAUU	GAUGCAAGCACUUGAAUUCAA	| Symbols: | Mannose-binding lectin s	14	0.813533491
AT4G34090.1_296	AT4G34090.1	296	1.914430747	3.018867925	2.466649336	3.06738962	4.721780604	3.894585112	ath-miR5636	3	1	21	308	328	CGUAGUUGCAGAGCUUGACGG	UCGUCAGGCUCUGUUACUGCG	| Symbols: | unknown protein; FUNC	12	1.57889695
AT2G39675.1_353	AT2G39675.1	353	2.205128205	2.6875	2.446314103	0	0	0	ath-miR173-5p	1.5	1	22	367	388	UUCGCUUGCAGAGAGAAAUCAC	GUGAUUUUUCUCUACAAGCGAA	| Symbols: TAS1C | TAS1C; other RN	14	0
AT1G76160.1_354	AT1G76160.1	354	2.466799658	2.348769899	2.407784778	1.839654721	1.610718273	1.725186497	ath-miR4221	1.5	1	22	366	387	UUUUCCUCUGUUGAAUUCUUGC	AAUGGAAUUCAACAGAGGAGGA	| Symbols: sks5 | SKU5 similar 5 | chi	12	0.716503615
AT2G25980.1_306	AT2G25980.1	306	1.788844622	2.951789627	2.370317124	0.984649123	2.403211418	1.693930271	ath-miR846	1.5	1	21	317	337	UUGAAUUGAAGUGCUUGAAUU	GAUCCAAGCACUUCAAUUCGA	| Symbols: | Mannose-binding lectin s	11	0.714642886
AT4G25210.1_566	AT4G25210.1	566	2.104575163	2.301438399	2.203006781	2.042553191	0.493297587	1.267925389	ath-miR864-3p	2	1	22	578	599	UAAAGUCAAUAAUACCUUGAAG	CUUCAAGGUAUUAUUGAUUUCA	| Symbols: | DNA-binding storekeeper	12	0.575543117
AT1G48410.2_498	AT1G48410.2	498	1.603753	2.694775435	2.149264218	1.140808344	4.707112971	2.923960657	ath-miR168a	3	1	21	511	531	UCGCUUGGUGCAGGUCGGGAA	UUCCCGAGCUGCAUCAAGCUA	| Symbols: AGO1 | Stabilizer of iron t	13	1.360447279
AT1G48410.3_508	AT1G48410.3	508	1.603753	2.694775435	2.149264218	1.140808344	4.707112971	2.923960657	ath-miR168a	3	1	21	521	541	UCGCUUGGUGCAGGUCGGGAA	UUCCCGAGCUGCAUCAAGCUA	| Symbols: AGO1 | Stabilizer of iron t	13	1.360447279
AT1G48410.1_498	AT1G48410.1	498	1.603497268	2.688656771	2.146077019	1.14235884	4.702363147	2.922360994	ath-miR168a	3	1	21	511	531	UCGCUUGGUGCAGGUCGGGAA	UUCCCGAGCUGCAUCAAGCUA	| Symbols: AGO1 | Stabilizer of iron t	13	1.361722327
AT2G38770.1_3161	AT2G38770.1	3161	1.185388845	3.04233871	2.113863777	3.150313152	4.715625	3.932969076	ath-miR1886.2	3	1	21	3173	3193	UGAGAUGAAAUCUUUGAUUGG	CCGUUCAAAGAUUUCUUCUCA	| Symbols: EMB2765 | P-loop contain	12	1.860559379
AT5G20580.1_1170	AT5G20580.1	1170	2.468085106	1.714285714	2.09118541	2.11550152	5.272727273	3.694114396	ath-miR394a	3	1	20	1184	1203	UUGGCAUUCUGUCCACCUCC	GGAGGUGGAGAGAAUAUCAA	| Symbols: | BEST Arabidopsis thaliar	14	1.766516913
AT2G44620.1_103	AT2G44620.1	103	2.157655382	1.91840204	2.038028711	2.504757136	2.296470588	2.400613862	ath-miR869.1	3	1	21	116	136	AUUGGUUCAAUUCUGGUGUUG	AAACCCUAGGAUUGAAUCAGU	| Symbols: MTACP-1, MTACP1 | mi	13	1.177909737
AT5G20580.2_1170	AT5G20580.2	1170	2.391752577	1.629976581	2.010864579	2.005763689	5.155555556	3.580659622	ath-miR394a	3	1	20	1184	1203	UUGGCAUUCUGUCCACCUCC	GGAGGUGGAGAGAAUAUCAA	| Symbols: | BEST Arabidopsis thaliar	14	1.780656768
AT3G22890.1_430	AT3G22890.1	430	2.044714325	1.964035411	2.004374868	3.519797276	2.04415011	2.781973693	ath-miR395a	3	1	21	442	462	CUGAAGUGUUUGGGGGAACUC	GAGUUCCUCCAAACUCUUCAU	| Symbols: APS1 | ATP sulfurylase 1	12	1.387950796
AT1G23390.1_518	AT1G23390.1	518	1.15542522	2.563673545	1.859549383	2.18466731	1.214977974	1.699822642	ath-miR775	3	1	20	531	550	UUCGAUGUCUAGCAGUGCCA	UGGAGCUGUUCGACAUCGAA	| Symbols: | Kelch repeat-containing F	13	0.914104598
AT2G39700.1_736	AT2G39700.1	736	3.347322721	0.235779817	1.791551269	0.463480613	0.273404255	0.368442434	ath-miR865-3p	3	1	21	747	767	UUUUUCCUCAAAUUUAUCCAA	UUGGAUGAGUUUGAGCAGAAA	| Symbols: ATEXPA4, ATEXP4, AT	11	0.205655535
AT4G35230.1_375	AT4G35230.1	375	2.534653465	0.947271045	1.740962255	1.226347305	3.531034483	2.378690894	ath-miR830-5p	3	1	22	388	409	UCUUCUCCAAAUAGUUUAGGUU	AGCCUAAACAAUUUGCGGAAGA	| Symbols: BSK1 | BR-signaling kinas	13	1.366308136
AT4G25210.1_567	AT4G25210.1	567	1.199674002	2.07	1.634837001	0.678341014	1.483870968	1.081105991	ath-miR864-3p	2	1	22	578	599	UAAAGUCAAUAAUACCUUGAAG	CUUCAAGGUAUUAUUGAUUUCA	| Symbols: | DNA-binding storekeeper	11	0.661292832
AT2G36380.1_859	AT2G36380.1	859	0.501207313	2.745209177	1.623208245	1.342883549	0.602404643	0.972644096	ath-miR773b-3p	2.5	1	21	871	891	UUUGAUUCCAGCUUUUGUCUC	GAGAGAGAAGCUGGAAUUAAG	| Symbols: PDR6, ATPDR6 | pleiotro	12	0.599210914
AT5G43780.1_383	AT5G43780.1	383	1.15354884	1.945519912	1.549534376	1.486922061	2.04505814	1.7659901	ath-miR395a	1.5	1	21	395	415	CUGAAGUGUUUGGGGGAACUC	GAGUUCCUCCAAACACUUCAU	| Symbols: APS4 | Pseudouridine synt	12	1.139690818
AT1G02130.1_140	AT1G02130.1	140	1.957569913	0.776587605	1.367078759	1.096309631	0.531413613	0.813861622	ath-miR5020a	3	1	21	152	172	UGGAAGAAGGUGAGACUUGCA	GGCAAGUCUUGUCUUCUUUUG	| Symbols: ATRAB1B, ARA5, ARA-	12	0.595328994
AT2G44620.1_102	AT2G44620.1	102	0.976976977	1.39399069	1.185483833	0.783209877	0.56612529	0.674667583	ath-miR869.1	3	1	21	116	136	AUUGGUUCAAUUCUGGUGUUG	AAACCCUAGGAUUGAAUCAGU	| Symbols: MTACP-1, MTACP1 | mi	14	0.569107367
AT1G77330.1_625	AT1G77330.1	625	1.237449615	1.105039267	1.171244441	1.815672745	1.601274993	1.708473869	ath-miR3933	2.5	1	21	639	659	AGAAGCAAAAUGACGACUCGG	AGGAGGUGUCGUUUUGCUUUU	| Symbols: | 2-oxoglutarate (2OG) and	14	1.458682585
AT1G35420.2_359	AT1G35420.2	359	1.891891892	0.343886463	1.117889177	2.154582763	0.837765957	1.49617436	ath-miR4228	2.5	1	21	371	391	AUAGCCUUGAACGCCGUCGUU	GUUGACGGUGUUGAAGGUUAU	| Symbols: | alpha/beta-Hydrolases su	12	1.338392383
AT4G24090.1_838	AT4G24090.1	838	0.447024673	1.788617886	1.11782128	2.298507463	3.5	2.899253731	ath-miR2112-5p	2.5	1	21	850	870	CGCAAAUGCGGAUAUCAAUGU	GUCUUGAUAUUUGCGUUUGCG	| Symbols: | unknown protein; FUNC	12	2.593664823
AT3G55620.1_634	AT3G55620.1	634	0.957966764	1.237854644	1.097910704	0.258166491	1.272255193	0.765210842	ath-miR776	2.5	1	21	648	668	UCUAAGUCUUCUAUUGAUGUU	CACCUCAGUGGAAGACUUGGA	| Symbols: emb1624 | Translation initi	14	0.696970017
AT3G13470.1_315	AT3G13470.1	315	0.778745645	1.38841435	1.083579997	1.12090274	1.271873666	1.196388203	ath-miR833b	3	1	21	326	346	UGUUUGUUGACAUCGGUCUAG	UCAGACUGGUGUUAACAAGCU	| Symbols: | TCP-1/cpn60 chaperonin	11	1.104106948
AT1G35420.1_293	AT1G35420.1	293	1.815519766	0.332261522	1.073890644	2.06391478	0.809399478	1.436657129	ath-miR4228	2.5	1	21	305	325	AUAGCCUUGAACGCCGUCGUU	GUUGACGGUGUUGAAGGUUAU	| Symbols: | alpha/beta-Hydrolases su	12	1.337805797
AT2G23610.1_823	AT2G23610.1	823	1.439781022	0.684895833	1.062338428	2.57122905	1.765100671	2.168164861	ath-miR5595a	2	1	21	836	856	ACAUAUGAUCUGCAUCUUUGC	UCAAAGACGCAGAUCAUAUGC	| Symbols: ATMES3, MES3 | methyl	13	2.040936113
AT5G25752.1_155	AT5G25752.1	155	1.34939759	0.602150538	0.975774064	5.78313253	2.028985507	3.906059019	ath-miR5653	3	1	24	169	191	UGGGUUGAGUUGAGUUGAGUUGG	GCCAACU-AACUCAACUCAACCCC	| Symbols: ATRBL11, RBL11 | rhom	14	4.00303632
AT1G20950.1_569	AT1G20950.1	569	1.063433644	0.830711991	0.947072817	1.632583998	0.590952839	1.111768419	ath-miR397a	3	1	21	583	603	UCAUUGAGUGCAGCGUUGAUG	GGUUAACGCUGCACUCAAAGC	| Symbols: | Phosphofructokinase fam	14	1.173899618
AT1G20225.1_319	AT1G20225.1	319	0.546948357	1.245989305	0.896468831	0	1.123794212	0.561897106	ath-miR169g-3p	3	1	21	333	353	UCCGGCAAGUUGACCUUGGCU	UGCCACGUUCAAUUUGCUGGA	| Symbols: | Thioredoxin superfamily	14	0.626789339
AT4G30170.1_871	AT4G30170.1	871	0.624127095	1.124567474	0.874347285	0.983172622	0.860167622	0.921670122	ath-miR5657	3	1	21	884	904	UGGACAAGGUUAGAUUUGGUG	CGUCAGAUCAAAUCUUGUUCA	| Symbols: | Peroxidase family protein	13	1.054123617
AT4G34920.1_914	AT4G34920.1	914	0.728244275	0.98027127	0.854257772	0.903409091	0.297752809	0.60058095	ath-miR5665	3	1	21	928	948	UUGGUGGACAAGAUCUGGGAU	GUUGCAGAUUUUGUCCACUGA	| Symbols: | PLC-like phosphodiester	14	0.703044174
AT3G17185.1_206	AT3G17185.1	206	0.78125	0.919117647	0.850183824	0	0	0	ath-miR390a	3	1	21	217	237	AAGCUCAGGAGGGAUAGCGCC	GGUGUUAUCCUAUCUGAGCUU	| Symbols: TASIR-ARF, TAS3, ATT	11	0
AT5G26830.1_1294	AT5G26830.1	1294	0.83756645	0.852778446	0.845172448	0.417304297	0	0.208652148	ath-miR173-3p	3	1	21	1306	1326	UGAUUCUCUGUGUAAGCGAAA	GUUCGCUCAUAUAGAGAGUUA	| Symbols: | Threonyl-tRNA synthetas	12	0.246875237
AT4G22220.1_419	AT4G22220.1	419	0.504341261	1.121163683	0.812752472	2.36438152	1.343678161	1.854029841	ath-miR5654-3p	2.5	1	23	432	454	UGGAAGAUGCUUUGGGAUUUAUU	CCGAAAUCGCAAAGCAUCUUUCU	| Symbols: ISU1, ATISU1 | SufE/Nif	13	2.281174041
AT3G28200.1_658	AT3G28200.1	658	0.937288136	0.646878199	0.792083167	1.187969925	0.204795852	0.696382889	ath-miR5629	3	1	22	671	692	UUAGGGUAGUUAACGGAAGUUA	AAGCUUGUGCUAAUUACCCUAA	| Symbols: | Peroxidase superfamily p	13	0.879179002
AT3G62680.1_660	AT3G62680.1	660	0.742632368	0.801694414	0.772163391	0.680237612	0.625874825	0.653056219	ath-miR5595a	2.5	1	21	672	692	ACAUAUGAUCUGCAUCUUUGC	GCAAAGAUACAGAUUGUGUGU	| Symbols: PRP3, ATPRP3 | proline-r	12	0.845748745
AT1G76140.2_811	AT1G76140.2	811	0.349668874	1.128205128	0.738937001	2.312891114	1.508571429	1.910731271	ath-miR823	3	1	21	823	843	UGGGUGGUGAUCAUAUAAGAU	UUUUUCUAUGGUCGCUACCCA	| Symbols: | Prolyl oligopeptidase fam	12	2.585783725
AT1G76140.1_811	AT1G76140.1	811	0.342229875	1.098066298	0.720148087	2.266802444	1.486907731	1.876855087	ath-miR823	3	1	21	823	843	UGGGUGGUGAUCAUAUAAGAU	UUUUUCUAUGGUCGCUACCCA	| Symbols: | Prolyl oligopeptidase fam	12	2.606207142
AT2G36310.1_1038	AT2G36310.1	1038	0.79245283	0.631578947	0.712015889	1.817307692	0.939422181	1.378364937	ath-miR5652	3	1	21	1049	1069	UUGAAUGUGAAUGAAUCGGGC	GCCUGAUUUAUUCACAUAUAA	| Symbols: URH1 | uridine-ribohydrol	11	1.93586261
AT3G13470.1_312	AT3G13470.1	312	1.038779956	0.369612403	0.70419618	0.800214823	0.508098892	0.654156857	ath-miR833b	3	1	21	326	346	UGUUUGUUGACAUCGGUCUAG	UCAGACUGGUGUUAACAAGCU	| Symbols: | TCP-1/cpn60 chaperonin	14	0.928941218
AT4G09010.1_953	AT4G09010.1	953	0.757414999	0.63377724	0.695596119	1.02446184	0.306274682	0.665368261	ath-miR5630a	2	1	21	967	987	GCUAAGAGCGGUUCUGAUGGA	UGCAACAGAACAGCUCUUAGC	| Symbols: APX4, TL29 | ascorbate p	14	0.956543952
AT4G27700.1_538	AT4G27700.1	538	0.533878107	0.833377624	0.683627866	1.628597395	1.537757437	1.583177416	ath-miR835-3p	3	1	21	551	571	UGGAGAAGAUACGCAAGAAAG	CUUUCUUUGGUAUCUUCUCUG	| Symbols: | Rhodanese/Cell cycle con	13	2.315846816
AT5G25752.1_158	AT5G25752.1	158	1.34939759	0	0.674698795	1.901528014	2.028985507	1.96525676	ath-miR5653	3	1	24	169	191	UGGGUUGAGUUGAGUUGAGUUGG	GCCAACU-AACUCAACUCAACCCC	| Symbols: ATRBL11, RBL11 | rhom	11	2.91279127
AT1G01320.1_649	AT1G01320.1	649	0.547643234	0.723837912	0.635740573	0.11765091	1.133897022	0.625773966	ath-miR394a	3	1	20	661	680	UUGGCAUUCUGUCCACCUCC	GGAGGUGGAAAGAAUUCUAA	| Symbols: | Tetratricopeptide repeat (T	12	0.984322839
AT1G01320.2_656	AT1G01320.2	656	0.545149481	0.721728595	0.633439038	0.117057513	1.130583323	0.623820418	ath-miR394a	3	1	20	668	687	UUGGCAUUCUGUCCACCUCC	GGAGGUGGAAAGAAUUCUAA	| Symbols: | Tetratricopeptide repeat (T	12	0.98481524
AT1G16720.1_1829	AT1G16720.1	1829	0.964516129	0.279113186	0.621814657	1.287405813	1.188866799	1.238136306	ath-miR868-3p	3	1	21	1841	1861	CUUCUUAAGUGCUGAUAAUGC	GCUUUAUCUGUACUUGAGAAG	| Symbols: HCF173 | high chlorophyl	12	1.991166164
AT1G20950.1_572	AT1G20950.1	572	0.93030303	0.311253802	0.620778416	1.037913547	1.57840617	1.308159859	ath-miR397a	3	1	21	583	603	UCAUUGAGUGCAGCGUUGAUG	GGUUAACGCUGCACUCAAAGC	| Symbols: | Phosphofructokinase fam	11	2.107289533
AT2G46800.1_292	AT2G46800.1	292	0.511897106	0.724294813	0.61809596	0.394254581	1.199698568	0.796976575	ath-miR856	1	1	22	304	325	UAAUCCUACCAAUAACUUCAGC	GUUGAAGUUGUUGGUGGGAUUA	| Symbols: ZAT, ATMTP1, MTP1, Z	12	1.289405896
AT2G46800.2_412	AT2G46800.2	412	0.509277031	0.718735892	0.614006461	0.392698569	1.189835575	0.791267072	ath-miR856	1	1	22	424	445	UAAUCCUACCAAUAACUUCAGC	GUUGAAGUUGUUGGUGGGAUUA	| Symbols: ZAT, ATMTP1, MTP1, Z	12	1.288695025
AT4G02510.1_3727	AT4G02510.1	3727	0.461609337	0.749812921	0.605711129	3.706535142	1.501998668	2.604266905	ath-miR5644	3	1	20	3739	3758	GUGGGUUGCGGAUAACGGUA	UACCGAUAUCUGGAACCCAC	| Symbols: TOC159, TOC86, PPI2, T	12	4.299519657
AT3G55620.1_637	AT3G55620.1	637	0.238791423	0.951086957	0.59493919	0.258166491	1.272255193	0.765210842	ath-miR776	2.5	1	21	648	668	UCUAAGUCUUCUAUUGAUGUU	CACCUCAGUGGAAGACUUGGA	| Symbols: emb1624 | Translation initi	11	1.286200094
AT1G52070.1_342	AT1G52070.1	342	0.642365537	0.546875	0.594620268	0	0.184372256	0.092186128	ath-miR846	2.5	1	21	354	374	UUGAAUUGAAGUGCUUGAAUU	GAUGCAAGCACUUGAAUUCAA	| Symbols: | Mannose-binding lectin s	12	0.155033612
AT3G49010.5_60	AT3G49010.5	60	0.408484129	0.705736251	0.55711019	0.6109375	1.220373747	0.915655623	ath-miR5662	2.5	1	20	74	93	AGAGGUGACCAUUGGAGAUG	UAUCCCCAAUGGUCACUUCA	| Symbols: ATBBC1, BBC1, RSU2 |	14	1.643580821
AT1G20225.1_322	AT1G20225.1	322	0.273153576	0.829181495	0.551167535	1.243329776	0.373397436	0.808363606	ath-miR169g-3p	3	1	21	333	353	UCCGGCAAGUUGACCUUGGCU	UGCCACGUUCAAUUUGCUGGA	| Symbols: | Thioredoxin superfamily	11	1.466638643
AT3G09050.1_633	AT3G09050.1	633	1.09787234	0	0.54893617	2.291296625	1.675324675	1.98331065	ath-miR865-3p	3	1	21	645	665	UUUUUCCUCAAAUUUAUCCAA	UUGGCUGAGUUUGAGGAGAAG	| Symbols: | unknown protein; FUNC	12	3.613007774
AT3G49010.4_62	AT3G49010.4	62	0.385390428	0.688235294	0.536812861	0.592648731	1.193181818	0.892915274	ath-miR5662	2.5	1	20	76	95	AGAGGUGACCAUUGGAGAUG	UAUCCCCAAUGGUCACUUCA	| Symbols: ATBBC1, BBC1, RSU2 |	14	1.663364161
AT1G48410.2_500	AT1G48410.2	500	0.686723349	0.384122919	0.535423134	1.597826087	0.3125	0.955163043	ath-miR168a	3	1	21	511	531	UCGCUUGGUGCAGGUCGGGAA	UUCCCGAGCUGCAUCAAGCUA	| Symbols: AGO1 | Stabilizer of iron t	11	1.783940556
AT1G48410.3_510	AT1G48410.3	510	0.686723349	0.384122919	0.535423134	1.597826087	0.3125	0.955163043	ath-miR168a	3	1	21	521	541	UCGCUUGGUGCAGGUCGGGAA	UUCCCGAGCUGCAUCAAGCUA	| Symbols: AGO1 | Stabilizer of iron t	11	1.783940556
AT1G48410.1_500	AT1G48410.1	500	0.686612798	0.383251051	0.534931924	1.6	0.312183497	0.956091749	ath-miR168a	3	1	21	511	531	UCGCUUGGUGCAGGUCGGGAA	UUCCCGAGCUGCAUCAAGCUA	| Symbols: AGO1 | Stabilizer of iron t	11	1.787314806
AT5G18800.1_117	AT5G18800.1	117	0.121979287	0.919961427	0.520970357	0.671594509	0.30070922	0.486151864	ath-miR5656	3	1	21	131	151	ACUGAAGUAGAGAUUGGGUUU	AAACCCGAUCCCUACUUCGGC	| Symbols: | Cox19-like CHCH family	14	0.933166078
AT5G18800.2_116	AT5G18800.2	116	0.121979287	0.919961427	0.520970357	0.671594509	0.30070922	0.486151864	ath-miR5656	3	1	21	130	150	ACUGAAGUAGAGAUUGGGUUU	AAACCCGAUCCCUACUUCGGC	| Symbols: | Cox19-like CHCH family	14	0.933166078
AT3G49010.1_72	AT3G49010.1	72	0.362960063	0.653755391	0.508357727	0.568650984	1.146993318	0.857822151	ath-miR5662	2.5	1	20	86	105	AGAGGUGACCAUUGGAGAUG	UAUCCCCAAUGGUCACUUCA	| Symbols: ATBBC1, BBC1, RSU2 |	14	1.687438011
AT3G49010.2_62	AT3G49010.2	62	0.362960063	0.653755391	0.508357727	0.568650984	1.146993318	0.857822151	ath-miR5662	2.5	1	20	76	95	AGAGGUGACCAUUGGAGAUG	UAUCCCCAAUGGUCACUUCA	| Symbols: ATBBC1, BBC1, RSU2 |	14	1.687438011
AT3G49010.3_87	AT3G49010.3	87	0.362960063	0.653755391	0.508357727	0.568650984	1.146993318	0.857822151	ath-miR5662	2.5	1	20	101	120	AGAGGUGACCAUUGGAGAUG	UAUCCCCAAUGGUCACUUCA	| Symbols: ATBBC1, BBC1, RSU2 |	14	1.687438011
AT4G09010.1_956	AT4G09010.1	956	0.504578313	0.492739008	0.49865866	1.195790504	0.92043956	1.058115032	ath-miR5630a	2	1	21	967	987	GCUAAGAGCGGUUCUGAUGGA	UGCAACAGAACAGCUCUUAGC	| Symbols: APX4, TL29 | ascorbate p	11	2.121922502
AT1G69740.2_637	AT1G69740.2	637	0.506180106	0.467035951	0.486608028	0.281782438	1.18387414	0.732828289	ath-miR4221	2.5	1	22	650	671	UUUUCCUCUGUUGAAUUCUUGC	UGAAGAAUUCAACAGGGGAUGA	| Symbols: HEMB1 | Aldolase superfa	13	1.505993008
AT1G69740.1_681	AT1G69740.1	681	0.502806361	0.464212458	0.48350941	0.27928123	1.178543461	0.728912345	ath-miR4221	2.5	1	22	694	715	UUUUCCUCUGUUGAAUUCUUGC	UGAAGAAUUCAACAGGGGAUGA	| Symbols: HEMB1 | Aldolase superfa	13	1.507545315
AT1G66670.1_795	AT1G66670.1	795	0.275769746	0.638869745	0.457319745	0.232330827	0	0.116165414	ath-miR397a	3	1	21	809	829	UCAUUGAGUGCAGCGUUGAUG	GAUCGACGCUGUAAUCGAUGA	| Symbols: CLPP3, NCLPP3 | CLP pr	14	0.254013553
AT4G22220.1_418	AT4G22220.1	418	0.314856712	0.47866242	0.396759566	0.615781711	0.09526526	0.355523485	ath-miR5654-3p	2.5	1	23	432	454	UGGAAGAUGCUUUGGGAUUUAUU	CCGAAAUCGCAAAGCAUCUUUCU	| Symbols: ISU1, ATISU1 | SufE/Nif	14	0.896067834
AT4G17340.1_795	AT4G17340.1	795	0.270379884	0.5225624	0.396471142	0.218277066	0.425894378	0.322085722	ath-miR3440b-3p	2.5	1	21	806	826	UGGAUUGGUCAAGGGAAGCGU	AAGCUACCCUUGAUCAAUCCU	| Symbols: TIP2;2, DELTA-TIP2 | tor	11	0.812381251
AT1G52070.1_343	AT1G52070.1	343	0.401171676	0.312267658	0.356719667	0.433526012	0.646248535	0.539887273	ath-miR846	2.5	1	21	354	374	UUGAAUUGAAGUGCUUGAAUU	GAUGCAAGCACUUGAAUUCAA	| Symbols: | Mannose-binding lectin s	11	1.513477733
AT5G13630.2_3554	AT5G13630.2	3554	0.392292254	0.277216857	0.334754555	0.827455177	0.205307433	0.516381305	ath-miR395a	2	1	21	3567	3587	CUGAAGUGUUUGGGGGAACUC	GAGUUUUCUCAAACGCUUCAG	| Symbols: GUN5, CCH, CHLH, CCI	13	1.542566924
AT5G13630.1_3554	AT5G13630.1	3554	0.387302067	0.270180381	0.328741224	0.72603964	0.18559957	0.455819605	ath-miR395a	2	1	21	3567	3587	CUGAAGUGUUUGGGGGAACUC	GAGUUUUCUCAAACGCUUCAG	| Symbols: GUN5, CCH, CHLH, CCI	13	1.386560529
AT1G77330.1_626	AT1G77330.1	626	0.448830409	0.200326264	0.324578337	0.37650233	0.177098356	0.276800343	ath-miR3933	2.5	1	21	639	659	AGAAGCAAAAUGACGACUCGG	AGGAGGUGUCGUUUUGCUUUU	| Symbols: | 2-oxoglutarate (2OG) and	13	0.852799807
AT5G13630.2_3553	AT5G13630.2	3553	0.362107275	0.277216857	0.319662066	0.579104803	0.307986182	0.443545493	ath-miR395a	2	1	21	3567	3587	CUGAAGUGUUUGGGGGAACUC	GAGUUUUCUCAAACGCUUCAG	| Symbols: GUN5, CCH, CHLH, CCI	14	1.387544972
AT5G54810.1_450	AT5G54810.1	450	0.461916462	0.170846965	0.316381713	0.742789411	1.582491582	1.162640497	ath-miR5642a	3	1	20	461	480	UCUCGCGCUUGUACGGCUUU	GGAGCAUUACAGGCGCGAGA	| Symbols: TSB1, TRPB, TRP2, ATT	11	3.674803087
AT5G13630.1_3553	AT5G13630.1	3553	0.357501888	0.270180381	0.313841134	0.508147603	0.278418064	0.393282833	ath-miR395a	2	1	21	3567	3587	CUGAAGUGUUUGGGGGAACUC	GAGUUUUCUCAAACGCUUCAG	| Symbols: GUN5, CCH, CHLH, CCI	14	1.253127109
AT1G69740.2_639	AT1G69740.2	639	0.252941176	0.373547616	0.313244396	0.281782438	0.337585868	0.309684153	ath-miR4221	2.5	1	22	650	671	UUUUCCUCUGUUGAAUUCUUGC	UGAAGAAUUCAACAGGGGAUGA	| Symbols: HEMB1 | Aldolase superfa	11	0.988634295
AT1G77330.1_627	AT1G77330.1	627	0.224251278	0.400914136	0.312582707	0.301128004	0.354401154	0.327764579	ath-miR3933	2.5	1	21	639	659	AGAAGCAAAAUGACGACUCGG	AGGAGGUGUCGUUUUGCUUUU	| Symbols: | 2-oxoglutarate (2OG) and	12	1.048569135
AT1G69740.1_683	AT1G69740.1	683	0.251256281	0.3712898	0.311273041	0.27928123	0.336068777	0.307675003	ath-miR4221	2.5	1	22	694	715	UUUUCCUCUGUUGAAUUCUUGC	UGAAGAAUUCAACAGGGGAUGA	| Symbols: HEMB1 | Aldolase superfa	11	0.988440896
AT1G23390.1_517	AT1G23390.1	517	0.247021944	0.364207802	0.305614873	0.094484412	0.867077465	0.480780939	ath-miR775	3	1	20	531	550	UUCGAUGUCUAGCAGUGCCA	UGGAGCUGUUCGACAUCGAA	| Symbols: | Kelch repeat-containing F	14	1.573159494
AT2G44620.1_104	AT2G44620.1	104	0.24278607	0.30704698	0.274916525	0	0.188126446	0.094063223	ath-miR869.1	3	1	21	116	136	AUUGGUUCAAUUCUGGUGUUG	AAACCCUAGGAUUGAAUCAGU	| Symbols: MTACP-1, MTACP1 | mi	12	0.342151942
AT2G20260.1_119	AT2G20260.1	119	0.226487997	0.276874116	0.251681057	0.124882556	0.382161187	0.253521871	ath-miR5631	2.5	1	21	131	151	UGGCAGGAAAGACAUAAUUUU	ACCAUUGUGUCUUUCUUGCCG	| Symbols: PSAE-2 | photosystem I su	12	1.007314078
AT5G43780.1_382	AT5G43780.1	382	0.493684211	0	0.246842105	0.742284358	0.679710145	0.710997251	ath-miR395a	1.5	1	21	395	415	CUGAAGUGUUUGGGGGAACUC	GAGUUCCUCCAAACACUUCAU	| Symbols: APS4 | Pseudouridine synt	13	2.88037266
AT4G27700.1_540	AT4G27700.1	540	0.07611281	0.415915119	0.246013965	0	0.38247012	0.19123506	ath-miR835-3p	3	1	21	551	571	UGGAGAAGAUACGCAAGAAAG	CUUUCUUUGGUAUCUUCUCUG	| Symbols: | Rhodanese/Cell cycle con	11	0.777334165
AT4G17340.1_792	AT4G17340.1	792	0.202730099	0.245639892	0.224184995	0.291120815	0.170183799	0.230652307	ath-miR3440b-3p	2.5	1	21	806	826	UGGAUUGGUCAAGGGAAGCGU	AAGCUACCCUUGAUCAAUCCU	| Symbols: TIP2;2, DELTA-TIP2 | tor	14	1.028848102
AT5G13180.1_807	AT5G13180.1	807	0.329842932	0.116236162	0.223039547	0.348869405	0.489954634	0.419412019	ath-miR1886.3	1	1	21	821	841	AAUUAAAGAUUUCAUCUUACU	UUUCAGAUGAAAUCUUUAAUU	| Symbols: ANAC083, VNI2, NAC0	11	1.880437907
AT1G74260.1_3345	AT1G74260.1	3345	0	0.436008677	0.218004338	3.378962536	1.834419817	2.606691177	ath-miR828	2.5	1	22	3357	3378	UCUUGCUUAAAUGAGUAUUCCA	GGGAUUACUCAUUUGAGUGAGA	| Symbols: PUR4 | purine biosynthesis	12	11.95706102
AT1G64150.1_570	AT1G64150.1	570	0.4342723	0	0.21713615	2.182890855	0	1.091445428	ath-miR835-3p	3	1	21	583	603	UGGAGAAGAUACGCAAGAAAG	CUUUCUUGCUUAUCUUUUUCU	| Symbols: | Uncharacterized protein fa	13	5.026548673
AT5G43060.1_495	AT5G43060.1	495	0.346297681	0.034603886	0.190450784	0.21304988	0.16722851	0.190139195	ath-miR396a	2	1	21	508	528	UUCCACAGCUUUCUUGAACUG	AAGAUCAAGGAAGCUGUGGGA	| Symbols: | Granulin repeat cysteine p	13	0.99836394
AT5G43060.1_495	AT5G43060.1	495	0.346297681	0.034603886	0.190450784	0.21304988	0.16722851	0.190139195	ath-miR396b	2	1	21	508	528	UUCCACAGCUUUCUUGAACUU	AAGAUCAAGGAAGCUGUGGGA	| Symbols: | Granulin repeat cysteine p	13	0.99836394
AT3G49010.5_63	AT3G49010.5	63	0.135919455	0.234524231	0.185221843	0.185422438	0.207833371	0.196627904	ath-miR5662	2.5	1	20	74	93	AGAGGUGACCAUUGGAGAUG	UAUCCCCAAUGGUCACUUCA	| Symbols: ATBBC1, BBC1, RSU2 |	11	1.061580542
AT3G49010.4_65	AT3G49010.4	65	0.128301887	0.228896945	0.178599416	0.180007563	0.203558956	0.191783259	ath-miR5662	2.5	1	20	76	95	AGAGGUGACCAUUGGAGAUG	UAUCCCCAAUGGUCACUUCA	| Symbols: ATBBC1, BBC1, RSU2 |	11	1.073817956
AT3G49010.1_75	AT3G49010.1	75	0.12084474	0.217458384	0.169151562	0.172735985	0.195724466	0.184230225	ath-miR5662	2.5	1	20	86	105	AGAGGUGACCAUUGGAGAUG	UAUCCCCAAUGGUCACUUCA	| Symbols: ATBBC1, BBC1, RSU2 |	11	1.089142914
AT3G49010.2_65	AT3G49010.2	65	0.12084474	0.217458384	0.169151562	0.172735985	0.195724466	0.184230225	ath-miR5662	2.5	1	20	76	95	AGAGGUGACCAUUGGAGAUG	UAUCCCCAAUGGUCACUUCA	| Symbols: ATBBC1, BBC1, RSU2 |	11	1.089142914
AT3G49010.3_90	AT3G49010.3	90	0.12084474	0.217458384	0.169151562	0.172735985	0.195724466	0.184230225	ath-miR5662	2.5	1	20	101	120	AGAGGUGACCAUUGGAGAUG	UAUCCCCAAUGGUCACUUCA	| Symbols: ATBBC1, BBC1, RSU2 |	11	1.089142914
AT4G30170.1_870	AT4G30170.1	870	0.226678291	0.101912825	0.164295558	0.736822218	0.286217525	0.511519872	ath-miR5657	3	1	21	884	904	UGGACAAGGUUAGAUUUGGUG	CGUCAGAUCAAAUCUUGUUCA	| Symbols: | Peroxidase family protein	14	3.113412664
AT4G17340.1_794	AT4G17340.1	794	0.135116876	0.184184676	0.159650776	0.072716696	0	0.036358348	ath-miR3440b-3p	2.5	1	21	806	826	UGGAUUGGUCAAGGGAAGCGU	AAGCUACCCUUGAUCAAUCCU	| Symbols: TIP2;2, DELTA-TIP2 | tor	12	0.227736744
AT2G21530.1_78	AT2G21530.1	78	0.168480451	0.127594628	0.14803754	0.413998019	0	0.20699901	ath-miR5658	0	1	21	89	109	AUGAUGAUGAUGAUGAUGAAA	UUUCAUCAUCAUCAUCAUCAU	| Symbols: | SMAD/FHA domain-con	11	1.398287288
AT3G62680.1_659	AT3G62680.1	659	0.117023928	0.153853716	0.135438822	0.090527838	0.06247505	0.076501444	ath-miR5595a	2.5	1	21	672	692	ACAUAUGAUCUGCAUCUUUGC	GCAAAGAUACAGAUUGUGUGU	| Symbols: PRP3, ATPRP3 | proline-r	13	0.564841327
AT1G69740.2_638	AT1G69740.2	638	0.05056444	0.140004341	0.095284391	0.234793054	0.084346803	0.159569929	ath-miR4221	2.5	1	22	650	671	UUUUCCUCUGUUGAAUUCUUGC	UGAAGAAUUCAACAGGGGAUGA	| Symbols: HEMB1 | Aldolase superfa	12	1.674670188
AT1G69740.1_682	AT1G69740.1	682	0.050227777	0.139158576	0.094693177	0.232709168	0.083967975	0.158338571	ath-miR4221	2.5	1	22	694	715	UUUUCCUCUGUUGAAUUCUUGC	UGAAGAAUUCAACAGGGGAUGA	| Symbols: HEMB1 | Aldolase superfa	12	1.67212229
AT3G49010.5_62	AT3G49010.5	62	0.045279669	0.108152686	0.076716177	0.052932019	0.034599729	0.043765874	ath-miR5662	2.5	1	20	74	93	AGAGGUGACCAUUGGAGAUG	UAUCCCCAAUGGUCACUUCA	| Symbols: ATBBC1, BBC1, RSU2 |	12	0.570490804
AT3G49010.4_64	AT3G49010.4	64	0.042749371	0.105580954	0.074165163	0.051398337	0.033898305	0.042648321	ath-miR5662	2.5	1	20	76	95	AGAGGUGACCAUUGGAGAUG	UAUCCCCAAUGGUCACUUCA	| Symbols: ATBBC1, BBC1, RSU2 |	12	0.575045204
AT3G11120.1_80	AT3G11120.1	80	0.076103501	0.065019506	0.070561503	0.287162162	0.162601626	0.224881894	ath-miR831	2.5	1	22	94	115	UGAUCUCUUCGUACUCUUCUUG	GAAGAAGCGUAUGAGGAGAUUA	| Symbols: | Ribosomal protein L41 fa	14	3.187033773
AT3G49010.1_74	AT3G49010.1	74	0.040265833	0.100308391	0.070287112	0.049323596	0.032594937	0.040959267	ath-miR5662	2.5	1	20	86	105	AGAGGUGACCAUUGGAGAUG	UAUCCCCAAUGGUCACUUCA	| Symbols: ATBBC1, BBC1, RSU2 |	12	0.582742203
AT3G49010.2_64	AT3G49010.2	64	0.040265833	0.100308391	0.070287112	0.049323596	0.032594937	0.040959267	ath-miR5662	2.5	1	20	76	95	AGAGGUGACCAUUGGAGAUG	UAUCCCCAAUGGUCACUUCA	| Symbols: ATBBC1, BBC1, RSU2 |	12	0.582742203
AT3G49010.3_89	AT3G49010.3	89	0.040265833	0.100308391	0.070287112	0.049323596	0.032594937	0.040959267	ath-miR5662	2.5	1	20	101	120	AGAGGUGACCAUUGGAGAUG	UAUCCCCAAUGGUCACUUCA	| Symbols: ATBBC1, BBC1, RSU2 |	12	0.582742203
AT2G20260.1_118	AT2G20260.1	118	0.08336071	0.030711663	0.057036186	0.090802348	0.080287929	0.085545139	ath-miR5631	2.5	1	21	131	151	UGGCAGGAAAGACAUAAUUUU	ACCAUUGUGUCUUUCUUGCCG	| Symbols: PSAE-2 | photosystem I su	13	1.499839733
AT2G20260.1_117	AT2G20260.1	117	0.047622958	0.040951776	0.044287367	0.090802348	0.02006365	0.055432999	ath-miR5631	2.5	1	21	131	151	UGGCAGGAAAGACAUAAUUUU	ACCAUUGUGUCUUUCUUGCCG	| Symbols: PSAE-2 | photosystem I su	14	1.251666185
AT3G22890.1_429	AT3G22890.1	429	0	0.085047759	0.04252388	0.437067338	0.611355634	0.524211486	ath-miR395a	3	1	21	442	462	CUGAAGUGUUUGGGGGAACUC	GAGUUCCUCCAAACUCUUCAU	| Symbols: APS1 | ATP sulfurylase 1	13	12.32746146

Supplementary Table 2. List of TAS3 homologs.

Species	TAS3 homolog	Accession	Clade	Cleavable (Yes/No)	nts between stop codon and the 5´ end of miR390 binding site	ORF length	aa length
Arabidopsis thaliana	TAS3a	AT3G17185	eudicots	No	6	153	50
Arabidopsis thaliana	TAS3b	AT5G49615	eudicots	No	10	129	42
Arabidopsis thaliana	TAS3c	AT5G57735	eudicots	No	9	150	49
Antirrhinum majus	TAS3	AJ797948.1	eudicots	No?	3	195	64
Burma mangrove	TAS3	BP947370.1	eudicots	No?	9	213	70
Glycine max	TAS3	BE330988.1	eudicots	No?	3	168	55
Gossypium raimondii	TAS3	CO077318.1	eudicots	Yes?	10	132	43
Manihot esculenta	TAS3	CK652751	eudicots	No?	3	102	33
Mesembryanthemum crystallinum	TAS3	BF479835.1	eudicots	No?	9	135	44
Populus trichocarpa	TAS3	DT498974.1	eudicots	No?	6	171	56
Solanum lycopersicum	TAS3-1	NR_138079.1	eudicots	No?	62	99	32
Solanum lycopersicum	TAS3-12	JX047547.1	eudicots	Yes?/No?	10	99	32
Swingle citrumelo	TAS3	CX663477.1	eudicots	No?	3	156	51
Theobroma cacao	TAS3	CA795323.1	eudicots	No?	3	114	37
Vitis vinifera	TAS3	DT025007.1	eudicots	No?	3	180	59
Pinus taeda	TAS3	DR112999.1	Gymnosperm	Yes	ORF	129	42
Hordeum vulgare	TAS3	BF264964.3	Monocots	Yes?	10	213	70
Oryza sativa Japonica	TAS3	AU100890.1	Monocots	No?	9	114	37
Saccharum	TAS3	CA145655.1	Monocots	Yes?	ORF	120	39
Sorghum bicolor	TAS3	CD464142.1	Monocots	No?	9	141	46
Triticum aestivum	TAS3	CN010916.1	Monocots	No?	9	177	58
Zea mays	TAS3	BE519095.1	Monocots	Yes?	14	126	41
Physcomitrella patens	TAS3a	BK005825	moss	Yes?	10	162	53
Physcomitrella patens	TAS3b	BK005826	moss	Yes?	nd		
Physcomitrella patens	TAS3c	BK005827	moss	Yes?	nd		
Physcomitrella patens	TAS3d	BK005828	moss	Yes?	nd		

? (predicted from sequence)

Supplementary Table 3. List of synthetic RNA oligos used in this study.

Name	Sequence (5′-3′)
miR390(21 nt)-guide	AAGCUCAGGAGGGAUAGCGCC(M)
miR390(21 nt)-passenger	CGCUAUCCAUCCUGAGUUUCA(M)
miR390(20 nt)-guide	AAGCUCAGGAGGGAUAGCGC(M)
miR390(20 nt)-passenger	GCUAUCCAUCCUGAGUUUCA(M)
miR390_21_4SU	AAGCUCAGGAGGGAUAGCGC4(M)
miR173(22 nt)-guide	UUCGCUUGCAGAGAGAAAUCAC(M)
miR173(22 nt)-passenger	GAUUCUCUGUGUAAGCGAACA(M)
miR173(21 nt)-guide	UUCGCUUGCAGAGAGAAAUCA(M)
miR173(21 nt)-passenger	AUUUCUCUCAGCAACGCAUAG(M)

"(M)" indicates 2′-OMe modification.

Supplementary Table 4. List of synthetic DNA oligos and long fragments used in this study.

Name	Sequence (5′-3′)
T7_ADH_5UTR_*3×HA*	ATGCCTGCAGGTCGACTCTAGATAATACGACTCACTATAGGGTACATCACAATCACACAAAACTAACAAAAGATCAAAAGCAAGTTCTTCACTGTTGATAatgGTTTACCCATACGATGTTCCTGACTATGCGGGCTATCCCTATGACGTCCCGGACTATGCAGGATCCTATCCATATGACGTTCCAGATTACGCTCCGTGGCGCGCCAGCTTGAGA
T7_TAS3a	CCGCGGTAATACGACTCACTATAGGATCCCACCGTTTCTTAAGACTCTCTCTCTTTCTGTTTTCTATTTCTCTCTCTCTCAAATGAAAGAGAGAGAAGAGCTCCCATGGATGAAATTAGCGAGACCGAAGTTTCTCCAAGGCATTAAGGAAAACATAACCTCCGTGATGCATAGAGATTATTGGATCCGCTGTGCTGAGACATTGAGTTTTTCTTCGGCATTCCAGTTTCAATGATAAAGCGGTGTTATCCTATCTGAGCTTTTAGTCGGATTTTTTCTTTTCAATTATTGTGTTTTATCTAGATGATGCATTTCATTATTCTCTTTTTCTTGACCTTGTAAGGCCTTTTCTTGACCTTGTAAGACCCCATCTCTTTCTAAACGTTTTATTATTTTCTCGTTTTACAGATTCTATTCTATCTCTTCTCAATATAGAATAGATATCTATCTCTACCTCTAATTCGTTCGAGTCATTTTCTCCTACCTTGTCTATCCCTCCTGAGCTAATCTCCACATATATCTTTTGTTTGTTATTGATGTATGGTTGACATAAATTCAATAAAGAAGTTGACGTTTTTCTCTCGAG
TAS3aPDS2	TTCATTTGGAGAGGCTCGAGGTCGACATCCCACCGTTTCTTAAGACTCTCTCTCTTTCTGTTTTCTATTTCTCTCTCTCTCAAATGAAAGAGAGAGAAGAGCTCCCATGGATGAAATTAGCGAGACCGAAGTTTCTCCAAGGTGATATGTCTATCTGTATATGTGATACGAAGAGTTAGGGTTTTGTCATTTCGAAGTCAATTTTTGTTTGTTTGTCAATAATGATATCTGAATGATGAAGAACACGTAACTAAGATATGTTACTGAACTATATAATACATATGTGTGTTTTTCTGTATCTATTTCTATATATATGTAGATGTAGTGTAAGTCTGTTATATAGACATTATTCATGTGTACATGCATTATACCAACATAAATTTGTATCAATACTACTTTTGATTTACGATGATGGATGTTCTTAGATATCTTCATACGTTTGTTTCCACATGTATTTACAACTACATATATATTTGGAATCACATATATACTTGATTATTATAGTTGTAAAGAGTAACAAGTTCTTTTTTCAGGCATTAAGGAAAACATAACCTCCGTGATGCATAGAGATTATTGGATCCGCTGTGCTGAGACATTGAGTTTTTCTTCGGCATTCCAGTTTCAATGATAAAGCGGTGTTATCCTATCTGAGCTTTTAGTCGGATTTTTTCTTTTCAATTATTGTGTTTTATCTAGATGATGCATTTCATTATTCTCTTTTAAGTAGCACTTCCCCACCTATTGAGAAGTGGGAACCCTAAAATCTCTTTCTAAACGTTTTATTATTTTCTCGTTTTACAGATTCTATTCTATCTCTTCTCAATATAGAATAGATATCTATCTCTACCTCTAATTCGTTCGAGTCATTTTCTCCTACCTTGTCTATCCCTCCTGAGCTAATCTCCACATATATCTTTTGTTTGTTATTGATGTATGGTTGACATAAATTCAATAAAGAAGTTGACGTTTTTCTACTAGTTCTAGACGCTGAAATCACCA
oligoK1	GAACAGATTGGAGGTATGAGTTCTAGGGCTGGTCCAATGTCTAA
oligoK2	CCATGGGACGTCGACCTGAGGTAATTATAACCCTCAATCATCTTCATTGTGAAGGCCATGCT
oligoE1	GCTGGCGCGCCATGGAAGAAAAAACTCATCATCATCATCAC
oligoE2	GCTGGCGCGCCTCAGCAGTAAAACATGAGATTCTTGAC
oligo512	CTTGTCATCGTCATCCTTGTAATCGATGTCATGATCTTTATAATCACCGTCATGGTCTTTGTAGTC
oligo955	TATAGGGAGACCCAAGCTGGCGCGCCATGGACTACAAAGACC
oligo1039	ACCTCCAATCTGTTCGCGGT
oligo1044	AACCACCTATCTACATCACCAAGATATGGGACATCATCATCATCATCACATGGACGAGAAGACCACCGG
oligo1062	CTCGCGAATGCATCTAGATCCGCGGTAATACGACTCACTATAGGA
oligo1063	TTGAGAGAGAGAGAAATAGA
oligo1064	GTTTTCTATTTCTCTCTCTCTCAAATGGACTACAAAGACCATGACGG
oligo1065	CGATTACAAGGATGACGATGACAAGATGAAAGAGAGAGAAGAGCTCC
oligo1066	GTCGACGGGCCCGGGATCCGATCTCGAGAGAAAAACGTCAACTTCTTTATTGAAT
oligo1073	TGGAGATTTCGAGTCGAGGGATAGACAAGGTAGGA
oligo1074	GACTCGAAATCTCCACATATATCTTTTGTTTGTTA
oligo1094	CCAAAAGTCTCAAGCTGGCGCGCCTCAGCAGTAGAACATGACAC
oligo1096	AAAAGTCTCAAGCTGGCGCGCCTCAGACGAAGAACATAACATTC
oligo1099	TTCGAGTCATAGGATAACACCGCTTTATCATTGAAACTGGAATG
oligo1100	ATCCTATGACTCGAATTAGTCGGATTTTTTCTTTTCAATT
oligo1101	AAGCTCAGATAGGATAACACGGCTTTATCATTGAAACTGGAATG
oligo1102	ATCCTATCTGAGCTTTTAGTCGGATTTTTTCTTTTCAATT
oligo1104	AAGCTCAGATAGGATAGCGCCGCTTTATCATTGAAACTGGAATG
oligo1106	ATCCCTCCTGAGCTTTTAGTCGGATTTTTTCTTTTCAATT
oligo1107	AAGCTCAGGAGGGATAGCGCCGCTTTATCATTGAAACTGGAATG
oligo1118	TATAGGGAGACCCAAGCTGGCGCGCCCCTGCAGGATGTACCCATACGATGTTCCAGATTACGCTTACCCATACGATGTTCCAGATTACGCTTACCCATACGATGTTCCAGATTACGCTATGGTGAGAAAGAGAAGAACGG
oligo1119	TATAGGGAGACCCAAGCTGGCGCGCCCCTGCAGGATGTACCCATACGATGTTCCAGATTACGCTTACCCATACGATGTTCCAGATTACGCTTACCCATACGATGTTCCAGATTACGCTATGGAGAGAGGTGGTTATCG
oligo1159	ACACCCAAAAGTCTCAAGCTGGCGCGCCTCAGCAGTAAAACATGAGAT
oligo1160	GGCTCACCGCGAACAGATTGGAGGTATGGAAGAAAAAACTCATCATCATC
oligo1161	TTTCAATGATAATTAAGCGGTGTTATCCTATCTGA
oligo1162	TAATTATCATTGAAACTGGAATGCCGAAGAAAAAC
oligo1163	TTCAATGATAAGTTAAGCGGTGTTATCCTATCTGA
oligo1164	TAACTTATCATTGAAACTGGAATGCCGAAGAAAAA
oligo1165	TCAATGATAAAGTTAAGCGGTGTTATCCTATCTGA
oligo1166	TAACTTTATCATTGAAACTGGAATGCCGAAGAAAA
oligo1167	CAATGATAACAGTTAAGCGGTGTTATCCTATCTGA
oligo1168	TAACTGTTATCATTGAAACTGGAATGCCGAAGAAA
oligo1180	AGTTTCAATGATAAAAGCGGTGTTATCCTATCTGA
oligo1181	TTTATCATTGAAACTGGAATGCCGAAGAAAAACTC
oligo1182	GTTTCAATGATAATAAGCGGTGTTATCCTATCTGA
oligo1183	TATTATCATTGAAACTGGAATGCCGAAGAAAAACT
oligo1197	TTCTCTCTCTCTCAAATGAAAGAGAGAGAAGAGCTCC
oligo1198	TTGAGAGAGAGAGAAATAGAAAACAG
oligo1201	GACTCTAGAGGATCCCCGGGTACCCTCGAGGTCGACATCCCACC
oligo1202	GAGAATAATGAAATGCATCATCTAG
oligo1203	CTAGATGATGCATTTCATTATTCTC
oligo1204	GGTGGGCGGCCGCTCTAGAACTAGTTAATTAAGAATTATCGAACCACTT
oligo1205	GATAGGATAACACCGCTTAACTGTTTATCATTGAAACTGGAATGCC
oligo1206	AACAGTTAAGCGGTGTTATCCTATCTGAGCTTTTA
oligo1207	CAGATAGGATAACACCGCTTAATTATCATTGAAACTGGAATGCC
oligo1208	TAATTAAGCGGTGTTATCCTATCTG
oligo1209	TTCGAGTCATAGGATAACACCGCTTTATCATTGAAACTGGAA
oligo1210	GCGGTGTTATCCTATGACTCGAATTAGTCGGATTTTTTCTTTTCA
oligo1211	TTATCACCATGGGAGCTCTTCTCTCT
oligo1212	AGAAGAGCTCCCATGGTGATAATTAGCGAGACCGAAGTTTCT
oligo1220	GCTTTATCATTGAAACTGGAATG
oligo1221	TTTCAATGATAAAGCAGTGTTATCCTATCTGAGCTT
oligoA1	AAACCTAAACCCCTAACGGC
oligoA2	TTACAATTTCAATATAAATGATATAATTTTTACA
oligoA3	AATTGGGCCCTCTAGATGCA
oligoA4	CACCGTCATGGTCTTTGTAGTCCATCTCACAAACTCGATCTCAATCTAGC
oligoA5	ATGGACTACAAAGACCATGAC
oligoA6	TAGACAGGGATATCGAACCTAACATCTTGTCATCGTCATCCTTGT
oligoA7	ATGTTAGGTTCGATATCCCTGTCTATTTGTC
oligoA8	GCTTGGTACCGAGCTCGGAT
oligoA9	TAATACGACTCACTATAGGGAAACCTAAACCCCTAACGGCTAAGC
oligoA10	TTTTTTTTTTTTTTTTTTTTTTTTTTTTTTTTTTTTTTTTTTTTTTTTTTTTTTTTTTTTGTAAAAATTATATCATTTATATTGAAATTGTAA
oligo1230	TCATTGAAACTGGAATGCCGAAGAAAAACTCAATGTCTCA
oligo1231	AAGAAAAACTCAATGTCTCAGCACAGCGGATCCAATAATC
oligo1232	GCACAGCGGATCCAATAATCTCTATGCATCACGGAGGTTA
oligo1233	TCTATGCATCACGGAGGTTATGTTTTCCTTAATGCCTTGG
oligo1234	TGTTTTCCTTAATGCCTTGGAGAAACTTCGGTCTCGCTAA
D7(+)_detection_probe	GGGGTCTTACAAGGTCAAGAA